Cell Reports

Article

Beyond pulsed inhibition: Alpha oscillations modulate attenuation and amplification of neural activity in the awake resting state

Graphical abstract

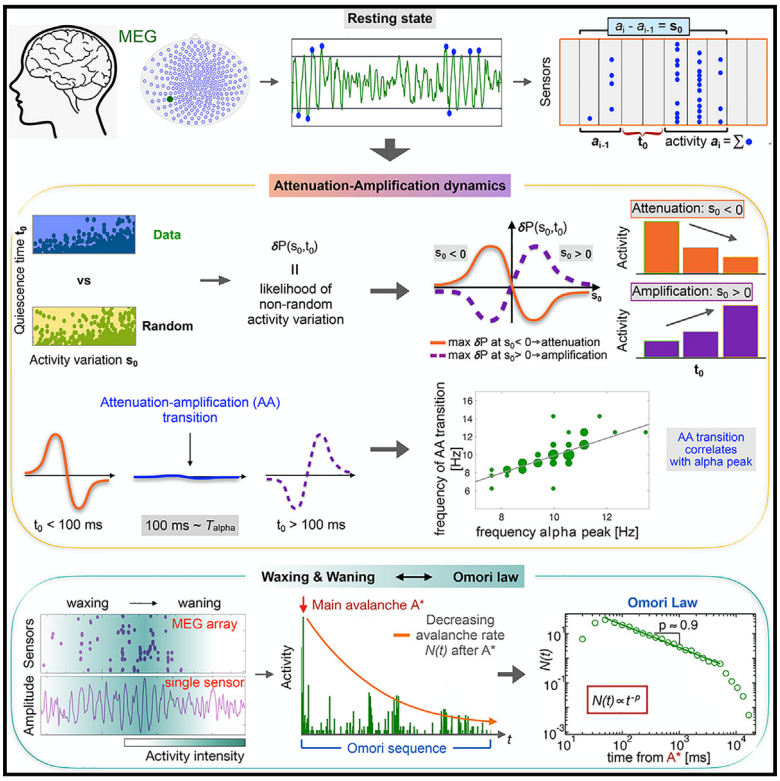

Highlights

- Resting-state brain activity displays attenuation-amplification dynamics (AADs)
- Attenuation occurs within single alpha cycles, amplification over a few alpha cycles
- Attenuation-amplification transitions correlate with individual alpha peak frequency
- Alpha "waxing and waning" is a long-term AAD that obeys the Omori law

Authors

Fabrizio Lombardi, Hans J. Herrmann, Liborio Parrino, ..., Anna Elisabetta Vaudano, Lucilla de Arcangelis, Oren Shriki

Correspondence

fabrizio.lombardi@ist.ac.at (F.L.), lucilla.dearcangelis@unicampania.it (L.d.A.), shrikio@bgu.ac.il (O.S.)

In brief

Alpha oscillations are considered to reflect cortical inhibition. However, the nature of such inhibition and the associated neural dynamics remain poorly understood. Lombardi et al. show that alpha oscillations modulate attenuation and amplification of resting-state activity, suggesting that alpha acts as a pacemaker for the alternation of inhibition and excitation.

Lombardi et al., 2023, Cell Reports *42*, 113162
October 31, 2023 © 2023 The Author(s).
https://doi.org/10.1016/j.celrep.2023.113162

CellPress

Cell Reports

CellPress
OPEN ACCESS

Article

Beyond pulsed inhibition: Alpha oscillations modulate attenuation and amplification of neural activity in the awake resting state

Fabrizio Lombardi,[1,2,14,*] Hans J. Herrmann,[3,4] Liborio Parrino,[5] Dietmar Plenz,[6] Silvia Scarpetta,[7,8] Anna Elisabetta Vaudano,[9,10] Lucilla de Arcangelis,[11,13,*] and Oren Shriki[12,13,*]

[1]Institute of Science and Technology Austria, Am Campus 1, 3400 Klosterneuburg, Austria
[2]Department of Biomedical Sciences, University of Padova, Via Ugo Bassi 58B, 35131 Padova, Italy
[3]Departamento de Fisica, Universitade Federal do Ceara, Fortaleza 60451-970, Ceara, Brazil
[4]PMMH, ESPCI, 7 quai St. Bernard, 75005 Paris, France
[5]Sleep Disorders Center, Department of Neurosciences, University of Parma, 43121 Parma, Italy
[6]Section on Critical Brain Dynamics, NIH, Bethesda, MD 20892, USA
[7]Department of Physics, University of Salerno, 84084 Fisciano, Italy
[8]INFN sez, Napoli Gr. Coll, 84084 Fisciano, Italy
[9]Neurology Unit, Azienda Ospedaliero-Universitaria of Modena, OCB Hospital, 41125 Modena, Italy
[10]Department of Biomedical, Metabolic, and Neural Sciences, University of Modena and Reggio Emilia, 41125 Modena, Italy
[11]Department of Mathematics and Physics, University of Campania "Luigi Vanvitelli", Viale Lincoln 5, 81100 Caserta, Italy
[12]Department of Cognitive and Brain Sciences, Ben-Gurion University of the Negev, Beer-sheva, Israel
[13]These authors contributed equally
[14]Lead contact
*Correspondence: fabrizio.lombardi@ist.ac.at (F.L.), lucilla.dearcangelis@unicampania.it (L.d.A.), shrikio@bgu.ac.il (O.S.)
https://doi.org/10.1016/j.celrep.2023.113162

SUMMARY

Alpha oscillations are a distinctive feature of the awake resting state of the human brain. However, their functional role in resting-state neuronal dynamics remains poorly understood. Here we show that, during resting wakefulness, alpha oscillations drive an alternation of attenuation and amplification bouts in neural activity. Our analysis indicates that inhibition is activated in pulses that last for a single alpha cycle and gradually suppress neural activity, while excitation is successively enhanced over a few alpha cycles to amplify neural activity. Furthermore, we show that long-term alpha amplitude fluctuations—the "waxing and waning" phenomenon—are an attenuation-amplification mechanism described by a power-law decay of the activity rate in the "waning" phase. Importantly, we do not observe such dynamics during non-rapid eye movement (NREM) sleep with marginal alpha oscillations. The results suggest that alpha oscillations modulate neural activity not only through pulses of inhibition (pulsed inhibition hypothesis) but also by timely enhancement of excitation (or disinhibition).

INTRODUCTION

The mammalian brain exhibits complex rhythmic dynamics that span a broad range of frequencies.[1] Brain rhythms emerge as periodic amplitude fluctuations in electrophysiological recordings, which result from synchronous activation of large populations of neurons.[2,3] Oscillations in distinct frequency bands have been associated with different brain functions and physiological states.[2,4,5] Among these brain rhythms, oscillations in the alpha band (8–13 Hz) play a prominent role in human brain activity. Characteristic of the eyes-closed, awake resting state, alpha oscillations have been associated with the processes of task disengagement,[6,7] perceptual learning and suppression of visual activity,[8,9] facilitation of periodic sampling of visual information, and, more generally, propagation of activity throughout the brain, modulation of communication between brain regions, and feedback processing within and across brain regions.[10–13] Indeed, a number of studies indicate that changes in cognitive performance are accompanied by rhythmic modulation of alpha amplitude and power, suggesting in particular an inverse relationship between alpha activity and neural firing.[6,8,14,15] Amplitude fluctuations occur across multiple timescales and show non-trivial features, such as long-range temporal correlations (LRTCs)[16,17] and non-Gaussian bimodal distributions of power,[18] which suggests the existence of two distinct modes: higher- and lower-power modes.[18] In particular, periodic fluctuations in amplitude, known as "waxing and waning," have long been considered a key feature of alpha oscillations.[19,20]

Several models have been proposed to explain the emergence of alpha oscillations and their dynamic characteristics, from mutually coupled excitatory (E) and inhibitory (I) spiking and stochastic neurons,[21,22] to adaptive neural networks[23] and more realistic thalamic and corticothalamic mechanistic models.[24–27] In particular, taking into account corticothalamic loop mechanisms, the

This is an open access article under the CC BY license (http://creativecommons.org/licenses/by/4.0/).

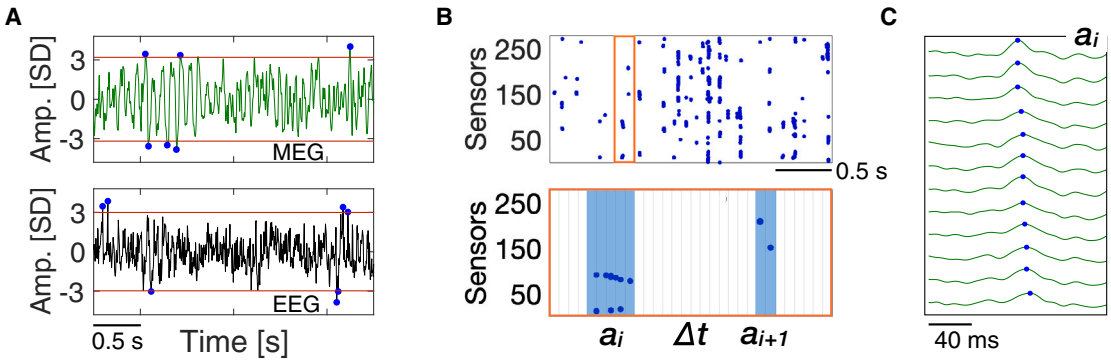

Figure 1. Neural activity cascades in the awake resting state

(A) Representative single-site MEG and EEG time series of resting-state activity in the human brain (top and bottom, respectively). Signals are z-normalized, and the amplitude (Amp.) is in units of standard deviation (SD) (STAR Methods). The most extreme point in each excursion beyond a threshold h (red lines) is treated as a discrete event (blue dots).

(B) Representative raster of discrete events across all MEG sensors (n = 273, top). An avalanche a_i is defined as a sequence of temporal windows ϵ ($\epsilon = 2T_{meg} = 3.3$ ms for the MEG; STAR Methods) with at least one event in any of the sensors, preceded and followed by at least one window with no events in any of the sensors (bottom). The same procedure is used for the EEG ($\epsilon = T_{eeg} = 4$ ms).

(C) Temporal sequence of events (blue dots) that belong to the avalanche a_i in (B), which spreads over 12 different sensors. Events are presented in time ascending order from top to bottom.

neural field model by Freyer et al.[26] reproduces spontaneous jumps between lower- and higher-power alpha modes in the presence of a subcritical Hopf bifurcation. Apart from the awake resting state, alpha oscillations can also be marginally observed in other physiologic states, such as rapid eye movement (REM) sleep and stage 1 of non-REM (NREM) sleep, or during electroencephalogram (EEG) arousals that may occur in REM and NREM sleep.[4,28,29]

Despite the advances in understanding the generation of the alpha rhythm and its influence on behavioral performance, the functional role of alpha oscillations in brain dynamics remains to a large extent not understood. Recent studies suggest that alpha oscillations mediate cortical inhibition. However, the nature of this inhibition, as well as its effects on collective neural dynamics, is still not known. One of the hypotheses that has recently gained consensus is that alpha-mediated inhibition is delivered in rhythmic pulses,[8,13,30,31] a mechanism that could allow selective information processing during periods of relative excitation.[32]

Directly verifying this hypothesis requires complex, simultaneous multiscale recordings of neural activity. However, we argue that it should be possible to identify the hallmarks of alpha-mediated, pulsed inhibition through analysis of neural dynamics that are readily accessible. To this end, we note that, within the pulsed inhibition hypothesis, alternating states of inhibition and excitation should result in periods of attenuation and enhancement of collective neural activity rhythmically modulated by alpha oscillations. To verify this assumption and, at the same time, to further clarify the functional role of the alpha rhythm in collective neural dynamics, we study neural activity cascades during resting wakefulness and NREM sleep, where alpha oscillations are only marginally present.[4,29] Neural activity cascades, termed neuronal avalanches, are spatiotemporal patterns of activity with no characteristic size, time, or spatial scale[33–37] that coexist with neural oscillations.[17,23,38–41] By dissecting the dynamics of neuronal avalanches in relation to the alpha rhythm, we show that alpha oscillations modulate bouts of neural activity attenuation and amplification unfolding over multiple timescales—from hundreds of milliseconds to seconds. This attenuation-amplification mechanism is not present during NREM sleep and suggests that the alpha rhythm mediates the timing of inhibition and excitation periods in the awake resting state. Importantly, our analysis provides a first quantitative description of the collective neural dynamics underlying the "waxing and waning" of the alpha rhythm.[18,19,42] We show that "waxing and waning" is a long-term mechanism for regulation of resting-state network excitability, which is intermittent rather than periodic in nature. The results suggest that, in the awake resting state, alpha oscillations modulate the intensity of neural activity not only through pulses of inhibition, as in the pulsed inhibition hypothesis, but also by timely enhancing excitation (or disinhibition), an effect that has not been described previously.

RESULTS

Dynamics of neural activity cascades during the awake resting state

To characterize collective brain dynamics in relation to the alpha rhythm, we analyzed magnetoencephalogram (MEG) and electroencephalogram (EEG) recordings of awake, eyes-closed, resting-state brain activity (STAR Methods). First, we proceeded to identify spatiotemporal cascades of neural activity across the sensor arrays. To this end, we mapped each continuous, broadband sensor signal into a sequence of discrete events. These are defined as the extremes of large positive and negative signal deflections exceeding an amplitude threshold h (Figure 1A). In practice, for each excursion beyond the threshold, a single event is identified at the most extreme value (maximum for positive excursions and minimum for negative excursions; blue dots in Figure 1A) (STAR Methods). This procedure preserves most of the

CellPress
OPEN ACCESS

collective features encoded in the continuous signals across the sensor array.[36,37,43]

In Figure 1B, we show a representative raster of events extracted from a MEG sensor array. The raster plot indicates that events tend to cluster in time across sensors or cortical locations. We define a neural activity cascade, or avalanche, a_i, as a sequence of consecutive time bins with at least one event in any of the sensors, preceded and followed by at least one empty time bin (Figures 1B, bottom, and 1C).[33] To each avalanche, we associate a size, s_i, which is given by the number of events occurring in the time bins that belong to it. It has been shown recently that the distribution $P(s)$ of avalanche sizes follows a power-law behavior—$P(s) \propto s^{-\tau}$—in MEG and EEG recordings.[17,36,37] Power-law distributions indicate an absence of characteristic scales, a property in stark contrast with the main essence of brain rhythms; namely, characteristic times and amplitudes.[1–3]

The scale-free power-law distribution of avalanche sizes does not suggest any potential link with neural oscillations. To characterize the dynamics of avalanches and identify relationships with coexisting rhythmic patterns, we turn our attention to the correlation properties of the cascading process. First, we analyze the autocorrelation function $C(t)$ of the quantity $n(t)$, the number of events occurring per unit time during the cascading process. We note that $n(t) = 0$ during quiet times, Δt, which correspond to periods with no threshold crossing events across the sensor array (Figure 1B, bottom). We find that $C(t)$ exhibits two distinct power-law regime for $t < 1$ s in MEG and EEG recordings (Figures 2A and 2B). At short timescales (regime ($A_<$)), $C(t)$ decays as $t^{-\gamma_<}$ with $\gamma_< \simeq 0.8$; for $120 < t < 1000$ ms (regime ($A_>$)), $C(t)$ shows a slower power law decay with $\gamma_> \simeq 0.2$ (Figures 2A–2B). Importantly, the crossover from regime ($A_<$) to regime ($A_>$) occurs around $t \simeq 100$ ms, which corresponds to the characteristic time of the alpha rhythm. The transition is preceded by a short plateau region between $20-100$ ms (Figures 2A and 2B). We observe that $C(t)$ exhibits a further transition to a slower-decaying regime around $t = 1$ s, which may be related to delta oscillations.

The transition between distinct scaling regimes indicates a change in the cascading dynamics at the temporal scale of the alpha rhythm.[46,47] We further investigate this point by analyzing the distribution of quiet times, $P(\Delta t)$ (Figures 2C and 2D). Indeed, power-law decays in the autocorrelation $C(t)$ can be related to power laws in the quiet time distribution.[46–48] In MEG and EEG data, we observe a close correspondence between short- and long-timescale regimes in $C(t)$ and $P(\Delta t)$, with the transition from one another occurring consistently around 100 ms. Such a correspondence, as well as the hallmark of alpha oscillations on $P(\Delta t)$ and $C(t)$, is particularly evident in the analysis of individual subjects (Figure S1). Specifically, for $\Delta t < 1$ s, $P(\Delta t)$ is well described by two distinct power-law regimes with exponents $\mu_<$ and $\mu_>$, which correspond to ($A_<$) and ($A_>$), defined in Figures 2A and 2B, for the autocorrelation $C(t)$. The crossover from one regime to the other is located around $\Delta t \simeq 100$ ms, as in $C(t)$ (Figures 2C and 2D; see also Figures S1–S3 for individual subjects and 40-min MEG). Thus, the regime ($A_<$) includes the quiet times that are shorter than a single alpha cycle (about 100 ms), while ($A_>$) includes the quiet times that span more than a single alpha cycle. This suggests that the change in the cascading dynamics marked by the crossover from ($A_<$) to ($A_<$) is closely connected to underlying properties of the alpha rhythm, as we shall investigate in the following sections. Such power-law regimes, ($A_<$) and ($A_>$), are followed by a faster decay of the probability $P(\Delta t)$ for Δts longer than 1 s.

Next, we analyze the conditional distributions $P(\Delta t | s > s_c)$, where s_c is a minimum threshold on avalanche sizes. In short, one only considers the Δts between consecutive avalanches of size $s > s_c$. We examine $P(\Delta t | s > s_c)$ for several s_c values. The analysis shows that, for $\Delta t \simeq 100$ ms, $P(\Delta t)$ is independent of s_c, while $P(\Delta t)$ depends on s_c for $\Delta t < 100$ ms and $\Delta t > 100$ ms (Figures S4 and S5). Specifically, for increasing s_c values, we find that (1) $P(\Delta t | s > s_c)$ decreases for $\Delta t < 100$ ms, and the exponent $\mu_<$ decreases and tends to zero, and (2) $P(\Delta t | s > s_c)$ increases for $\Delta t > 100$ ms and shows a power law with decreasing exponents (Figure S4). This shows that, in stark contrast to similar analyses in rats and zebrafish in the absence of alpha oscillations,[35,49] $\Delta t \simeq 100$ ms behaves as a fixed point for the transformation that selectively removes avalanches smaller than a threshold s_c, while the rest of the distribution changes. This further indicates that alpha oscillations play a key role in shaping the distribution of quiet times, thus determining the emergent dynamics of avalanches in the resting state.

The double power-law, non-exponential quiet time distribution as well as the autocorrelation $C(t)$ imply that neural cascades of activity are strongly correlated[37,50–54] and indicate that the nature of correlations in the cascading process depends on the time scales. Indeed, the distribution $P(\Delta t)$ calculated after random phase shuffling (STAR Methods) of the original brain signals is exponential (Figures 2C and 2D). Furthermore, we observe that, despite the analogies between avalanches and earthquakes,[54,55] the double power-law behavior in $P(\Delta t)$ does not arise from the non-homogeneity of the avalanche rate (Figure S6), as found for earthquakes instead.[56]

The observed functional behavior of $P(\Delta t)$ as well as the autocorrelation function $C(t)$ suggest that the relationship between consecutive avalanches (and, thus, the underlying collective neural dynamics) undergoes a transition around $\Delta t \simeq 100$ ms. Here, we hypothesize that this transition reflects a property of the neural dynamics associated with generation and propagation of the alpha rhythm in resting-state brain activity. To verify this hypothesis, we investigate whether the collective neural dynamics encoded in avalanche characteristics (e.g., their sizes) exhibit signatures of dynamic transitions that correlate with alpha oscillations.

Attenuation-amplification dynamics (AADs) of neural activity in the awake resting state

To this end, we consider the avalanche size increments $\Delta s = s_{i+1} - s_i$ between the size of avalanche a_i and the size of the subsequent avalanche a_{i+1} and analyze their relationship with the corresponding quiet times Δt_i (Figure 1). Negative values of Δs imply attenuation (i.e., the avalanche a_{i+1} is smaller than its preceding one, a_i), whereas positive values imply amplification; namely, the avalanche a_{i+1} is larger than the preceding avalanche a_i

We first examine the scatter plot between Δss and the corresponding Δts (Figures 2E and 2F). For $\Delta s < 0$, we observe that large negative Δss occur with short quiet-time Δts and vice versa

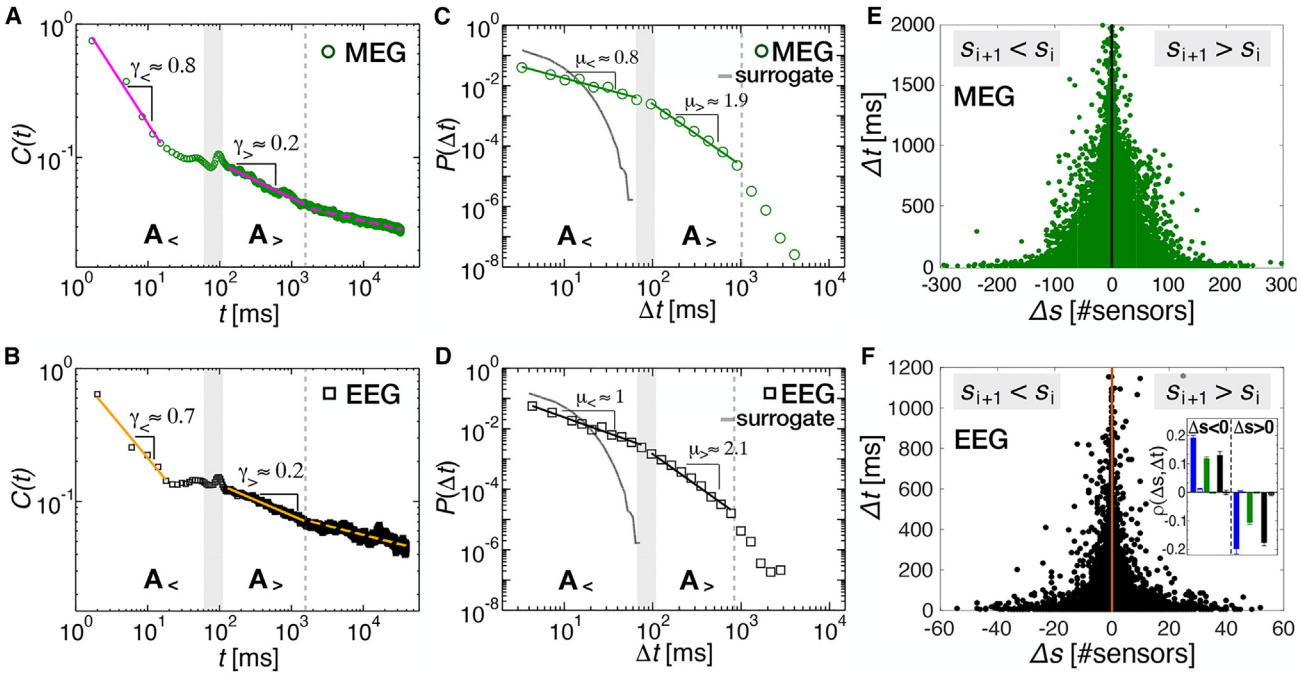

Figure 2. Transition in the dynamics of neural activity cascades at the timescale of the alpha rhythm during resting wakefulness

(A) Autocorrelation $C(t)$ of the network activity, $n(t)$, in 4-min MEG recordings. $n(t)$ is measured as the number of active sensors in each time bin ϵ. In the short timescales (regime ($A_<$)), $C(t)$ decays as a power law with an exponent $\gamma_< = 0.7633 \pm 0.0540$. After a transition region (20–120 ms), where $C(t)$ is nearly constant and shows a small peak at $t = 100$ ms, the autocorrelation follows a power law with an exponent $\gamma_> = 0.2619 \pm 0.0028$ (regime ($A_>$)).

(B) Autocorrelation $C(t)$ of the network activity for EEG recordings. Within regime ($A_<$), $C(t)$ decays as a power law with an exponent $\gamma_< = 0.6627 \pm 0.0990$, while within regime ($A_>$), the autocorrelation follows a power law with an exponent $\gamma_> = 0.2309 \pm 0.0019$.

(C) The distribution of quiet times $P(\Delta t)$ in 4-min MEG recordings (n = 70) shows a double power-law behavior with regime ($A_<$) for short Δts characterized by an exponent $\mu_< = 0.7897 \pm 0.0144$ and regime ($A_>$) for longer Δts with an exponent $\mu_> = 1.9690 \pm 0.0394$, followed by an exponential cutoff. The transition region (shaded area) between regime ($A_<$) and ($A_>$) is located around 100 ms. $P(\Delta t)$ from surrogate data (STAR Methods) shows an exponential behavior (gray curve). A similar behavior is observed in 40-min-long MEG recordings (Figure S3).

(D) The distribution of quiet times in EEG recordings (n = 6) of the awake resting state is consistent with the scenario described in (C): regime ($A_<$), $\mu_< = 1.0832 \pm 0.0544$; regime ($A_>$), $\mu_> = 2.0830 \pm 0.1514$. As in the MEG, the transition region (shaded area) is located at around 100 ms. $P(\Delta t)$ from surrogate data shows an exponential behavior (gray curve).

(E) Scatter plot between Δs and Δt for all MEG subjects. Negative Δss are positively correlated with their corresponding quiet times, whereas positive Δss are anti-correlated with their relative quiet times (Spearman's correlation coefficient: $\rho(\Delta s < 0, \Delta t) = 0.1916 \pm 0.0088$ and $\rho(\Delta s < 0, \Delta t) = 0.1188 \pm 0.0061$ in 40-min and 4-min MEG recordings, respectively; $\rho(\Delta s > 0, \Delta t) = -0.1064 \pm 0.0065$ in 4-min MEG, $\rho(\Delta s > 0, \Delta t) = -0.1985 \pm 0.0181$ in 40-min MEG).

(F) The scatter plot between Δs and Δt for all EEG subjects exhibits the same behavior as observed in the MEG ($\rho(\Delta s < 0, \Delta t) = 0.1301 \pm 0.0135$; $\rho(\Delta s > 0, \Delta t) = -0.1765 \pm 0.0111$). Inset: $\rho(\Delta s, \Delta t)$ calculated separately for $\Delta s < 0$ and $\Delta s > 0$ (blue, MEG 40 min; green, MEG 4 min; black, EEG). $\rho(\Delta s, \Delta t)$ from surrogate data are plotted next to each bar and are very close to zero in all cases. t tests comparing original and surrogate data show that correlations between Δs and Δt are significant ($p < 0.001$; STAR Methods). Distributions were calculated using $\epsilon = 2T_{meg} = 3.3$ ms and $\epsilon = 1T_{eeg} = 4$ ms for MEG and EEG data, respectively. Results are independent of ϵ (Figure S2). Power-law fits were performed using a maximum likelihood estimator and compared with exponential fits via log likelihood ratios (STAR Methods)[44,45] (MEG 4-min; regime $A_<$: $R = 395$, $p = 0.03$; regime $A_>$, $R = 346$, $p = 2 \cdot 10^{-18}$. EEG; regime $A_<$: $R = 567$, $p = 4 \cdot 10^{-33}$; regime $A_>$: $R = 72$, $p = 0.0003$). In all cases, the power law is more likely to describe the empirical data (STAR Methods). The p value measures the significance of R and is defined in the STAR Methods.

in MEG (Figure 2E) and EEG recordings (Figure 2F). The corresponding value of Spearman's correlation coefficient $\rho(\Delta s < 0, \Delta t)$ (STAR Methods) is significantly larger than zero (Figure 2F, inset), indicating that negative size increments are positively correlated with their corresponding quiet times; i.e., the more negative the increment, the shorter the quiet time separating two avalanches. In contrast, we find that positive size increments, $\Delta s > 0$, tend to be significantly anti-correlated with the corresponding quiet times in MEG and EEG data (Figure 2F, inset).

To dissect the dependency of size increments on the time lag separating consecutive avalanches and identify the connection with the alpha rhythm, we scrutinize the correlation landscape hidden in the density distribution across the $\Delta t \Delta s$ plane of the scatterplots shown in Figures 2E and 2F. To this aim, we systematically compare the spatial structure of the density in the plane $\Delta t \Delta s$ with surrogate densities obtained by randomly reshuffling avalanche sizes. In this way, the distribution and the temporal order of quiet times are preserved, as well as the size distribution (Figure 3A).

The local density distribution resulting from the avalanche process can be described using the conditional probability $P(s_0, t_0) \equiv P(\Delta s < s_0 | \Delta t < t_0) = N(\Delta s < s_0 | \Delta t < t_0)/N(\Delta t < t_0)$, where the thresholds s_0 and t_0 delimit the plane region $R(s_0, t_0)$

CellPress
OPEN ACCESS

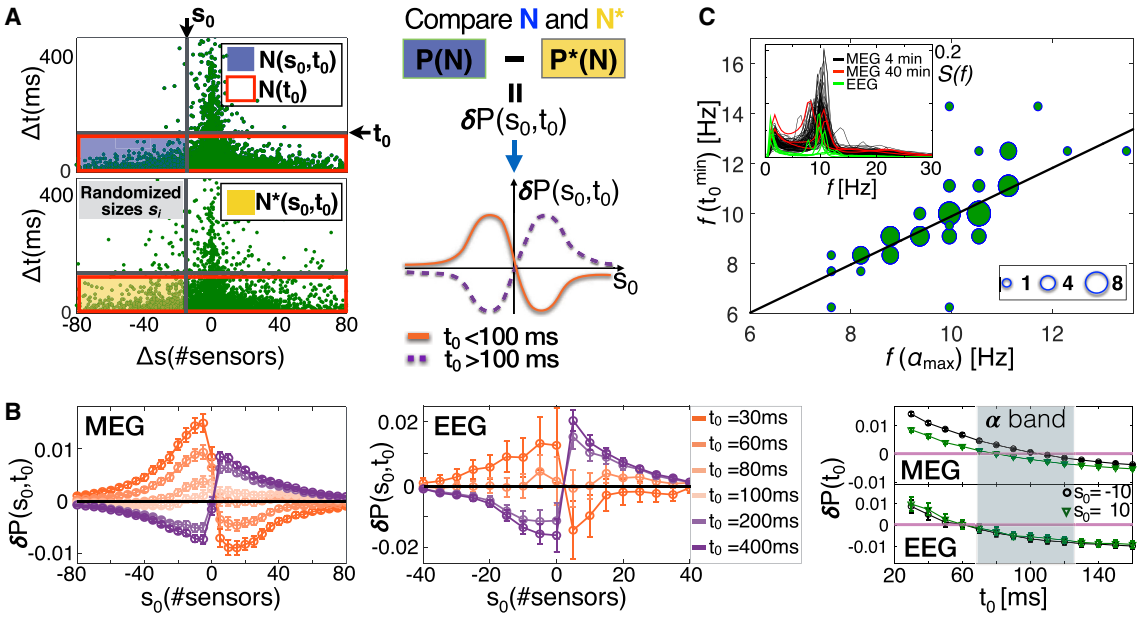

Figure 3. The monotonic relationship between consecutive avalanches undergoes a transition from an attenuation to an amplification regime that correlates with the characteristic time of the alpha rhythm

(A) Schematic definition of the quantity $\delta P(s_0,t_0) \equiv \delta P(\Delta s < s_0 | \Delta t < t_0)$. Left: the conditional probabilities $P(s_0,t_0)$ and the surrogate conditional probabilities $P^*(s_0,t_0)$ are proportional to the number of points $N(s_0,t_0)$ and $N^*(s_0,t_0)$ in the region $R(s_0,t_0)$ of the plane $\Delta s \Delta t$ defined by the thresholds s_0 and t_0 (blue and yellow rectangles, respectively). Top right: the quantity $\delta P(s_0,t_0)$ compares the original and the surrogate density in the region $R(s_0,t_0)$ of the plane and is defined as the difference between $P(s_0,t_0)$ and $P^*(s_0,t_0)$, the conditional probabilities associated with the density N and N^* for original and surrogate data (STAR Methods). Bottom right: the quantity $\delta P(s_0,t_0)$ as a function of s_0 for a given threshold t_0 on Δts exhibits two relevant scenarios. For $t_0 < 100$ ms (attenuation regime, orange thick line), $\delta P(s_0,t_0)$ has a maximum for $s_0 < 0$, implying that s_{i+1} tends to be smaller than s_i for $\Delta t < t_0$. For $t_0 > 100$ ms (amplification regime, purple dashed line), $\delta P(s_0,t_0)$ has a maximum for $s_0 > 0$, implying that, for $\Delta t < t_0$, s_{i+1} tends to be larger than s_i.

(B) $\delta P(s_0,t_0)$ as a function of the threshold s_0 on Δs for different values of the threshold t_0 on Δts for 4-min MEG (left, n = 70) and EEG (center, n = 6) data. The error bar on each data point is two times the SD σ^* associated with the surrogate $P^*(s_0,t_0)$ (STAR Methods). For a given t_0, the maximum in $\delta P(s_0,t_0)$ indicates the preferred relation between consecutive avalanches separated by quiet times shorter than t_0. In MEG and EEG recordings (left and center), for t_0 smaller than $\approx$ 100 ms, $\delta P(s_0,t_0)$ has a maximum at $s_0 < 0$, and, thus, an avalanche tends to be smaller than its preceding one ($s_{i+1} < s_i$, attenuation regime). On the contrary, for t_0 larger than $\approx$100 ms, the maximum moves toward positive s_0, implying that a given avalanche tends to be larger than the preceding one ($s_{i+1} > s_i$, amplification regime). For $t_0 \approx 100$ ms, $\delta P(s_0,t_0)$ is very close to zero for each s_0, indicating that, at $t_0 \simeq 100$ ms, there is not a preferred sign for Δs and that $\Delta t \simeq 100$ ms is a transition point from one dynamic regime to another—an attenuation-amplification transition. A similar behavior is observed in 40-min MEG recordings (Figure S7). Right: $\delta P(s_0,t_0)$ as a function of t_0 for $s_0 = -10$ and $s_0 = 10$ in 4-min MEG and EEG. For each s_0, $\delta P(t_0)$ transitions from positive to negative values in a range of t_0 corresponding to the alpha band ($\approx$80 ms and $\approx$130 ms). A similar behavior is observed in 40-min MEG (Figure S7).

(C) The scatter plot between $f(\alpha_{max})$ and $f(t_0^{min})$ shows that the attenuation-amplification transition in $\delta P(s_0,t_0)$ correlates with the maximum in the α band of the power spectrum. The size of each circle is proportional to the number of points (subjects) in the corresponding region of the plane. The black thick line is a linear fit, $Y = A \cdot X + B$, with $A = 0.96$ and $B = 0.26$ ($r^2 = 0.80$). Inset: power spectrum $S(f)$ for each subject (black lines, MEG 4 min; red lines, MEG 40 min; green lines, EEG).

under investigation (Figure 3A, top left, blue shaded area). An analogous quantity $P^*(s_0,t_0)$ can be associated with the surrogate region resulting from the size reshuffling procedure (Figure 3A, bottom left, yellow shaded area). The difference $\delta P(s_0,t_0) \equiv \delta P(\Delta s < s_0 | \Delta t < t_0) = P(s_0,t_0) - P^*(s_0,t_0)$ is a measure of the likelihood that a specific distribution of points in the region $R(s_0,t_0)$ results from the actual avalanche dynamics rather than from random avalanche occurrences and is used to examine the relationship between sizes of consecutive avalanches as a function of the quiet times separating them. We indicate with σ^* the standard deviation associated with the surrogates $P^*(s_0,t_0)$. Thus, if $|\delta P(s_0,t_0)| > 2\sigma^*$, then $P(s_0,t_0)$ and $P^*(s_0,t_0)$ are significantly different ($p < 0.05$; STAR Methods), and the distribution of points in the region $R(s_0,t_0)$ is considered to reflect a specific, non-random relationship between Δs and Δt.

We study $\delta P(s_0,t_0)$ as a function of s_0 for fixed t_0 values. For each fixed value of t_0, there are two possible relevant scenarios for the function $\delta P(s_0,t_0)$ (Figure 3A, right): (1) $\delta P(s_0,t_0)$ is positive and monotonically increases for $-\infty < s_0 < 0$, reaches a maximum, and then decreases, taking a minimum at some $s_0 > 0$ (Figure 3A, right, bottom, orange thick line). This is the *attenuation regime*, during which the size increments, $\Delta s = s_{i+1} - s_i$, tend to be negative, and the avalanche a_{i+1} tends to be smaller than the preceding avalanche a_i; (2) $\delta P(s_0,t_0)$ is negative and monotonically decreases for $-\infty < s_0 < 0$, reaches a minimum, and then increases, taking a local maximum at some $s_0 > 0$ (Figure 3A, right, bottom, purple dashed line). This is the *amplification regime*. In this dynamic regime, the size increments tend to be positive, and a given avalanche a_{i+1} tends to be larger than its preceding avalanche a_i. Following this approach, we

show that the attenuation and amplification regimes correspond to regimes ($A_<$) and ($A_>$) defined in Figure 2.

We first analyze $\delta P(s_0, t_0)$ as a function of s_0 for several fixed values of the threshold t_0 (Figure 3B). If the relation between consecutive avalanches depends on their distance in time, then $\delta P(s_0; t_0)$ changes as we consider different t_0 values. In Figure 3B, we show the function $\delta P(s_0, t_0)$ evaluated for t_0 values ranging between 30 and 1,000 ms. We find that $\delta P(s_0; t_0)$ follows the attenuation regime for t_0s smaller than approximately 100 ms, whereas it conforms to the amplification regime for larger t_0 values. Thus, size increments Δs tend to be negative when the quiet time between consecutive avalanches is shorter than 100 ms and positive otherwise. This behavior is also observed in 40-min MEG data (Figure S7) and is consistent across subjects (Figure S8). The tendency for negative Δss to be coupled with $\Delta t < 100$ ms implies that avalanche sizes preferentially exhibit a decreasing trend on short timescales, a clear sign of attenuated bursting activity. On the other hand, the significant likelihood of positive increments at longer timescales suggests the presence of a regulatory mechanism that, after discharging cycles with decreasing avalanche sizes, amplifies bursting activity and leads to the appearance of larger avalanches. The transition from the attenuation to the amplification regime occurs at $t_0 \approx 100$ ms, where we observe that $\delta P(s_0, t_0) \simeq 0$ (Figure 3B). Importantly, $\delta P(s_0, t_0) \simeq 0$ implies that $P(s_0, t_0) \simeq P^*(s_0, t_0)$, which, in turn, implies that, in the plane $\Delta t \Delta s$, the local density around $\Delta t \approx 100$ ms is comparable with the density obtained with the reshuffled avalanche sizes. Crucially, we observe that the attenuation and amplification regimes correspond to regime ($A_<$) and ($A_>$) in the quiet-time distributions and that the attenuation-amplification transition coincides with the crossover from regime ($A_<$) to regime ($A_>$) (Figures 2C and 2D).

The AAD of the awake resting state correlates with the alpha rhythm

To identify the transition point t_0^{min} from the attenuation to the amplification regime, we study $\delta P(\Delta s < s_0, \Delta t < t_0)$ as a function of t_0 for a range of fixed s_0 values; i.e., $\delta P(t_0)$ (Figure 3B, right). We plot $\delta P(t_0)$ for $s_0 = \pm 10$, where the quantity $\delta P(\Delta s < s_0, \Delta t < t_0)$ is generally non-zero away from the transition point (Figure 3, left and center panels). A similar behavior is observed for other s_0 values (Figure S7). We find that the transition from positive to negative $\delta P(t_0)$ lies mostly in the range [70 ms, 130 ms] (Figures 3B and S7), which approximately corresponds to oscillations in the frequency range of 8–13 Hz, commonly identified as the alpha band. Similar results are obtained in 40-min MEG recordings (Figure S7). Then we define t_0^{min} as the t_0 that minimizes $|\delta P(\Delta s < s_0 | \Delta t < t_0)|$ over a range of relevant s_0 values; namely $t_0^{min} = \min_{t_0}(\sum_{s_0=-30}^{30} |\delta P(\Delta s < s_0 | \Delta t < t_0)|)$.

Next, we show that the attenuation-amplification transition correlates with the timescale characteristic of the alpha rhythm and is consistent across subjects in MEG and EEG recordings of the awake resting state (Figures S7 and S8). In Figure 3C, for all subjects, we plot the frequency $f(\alpha_{max})$, which corresponds to the maximum power in the alpha band, versus the transition frequency $f(t_0^{min}) = 1/t_0^{min}$ corresponding to the transition point t_0^{min} from the attenuation regime to the amplification regime (Figure 3C). We observe that the frequency $f(t_0^{min})$ correlates with $f(\alpha_{max})$ ($r^2 = 0.80$), indicating that the attenuation-amplification transition is intimately connected to the dynamics of alpha oscillations. Importantly, the correlation between the transition frequency $f(t_0^{min})$ and $f(\alpha_{max})$ suggests that the crossover in the distribution of quiet times and in the quantity $\delta P(s_0, t_0)$ relates to a basic difference in the cascading process within and between alpha cycles.

Alpha "waxing and waning": A long-term mechanism that regulates attenuation and amplification bouts according to the Omori law

We have shown that the AAD of the resting state cascading process acts on a timescale of less than a second, with an attenuation-amplification transition that correlates with the characteristic frequency of alpha oscillations (Figure 3). Importantly, alpha waves are also known to exhibit long-term alternation between higher- and lower-amplitude fluctuations over timescales of several seconds—the so called "waxing and waning" phenomenon.[18–20] To characterize the resting-state cascading process in relation to alpha "waxing and waning," we focus on large cascades of activity, which we define as avalanches larger than a given size s^* and label them as main avalanches, A^* (Figure 4A, left top panel). Large avalanches are synchronous events consisting of time-clustered, higher-amplitude signal fluctuations over a large number of sensors (see the raster plot in Figure 4A, left bottom panel). We observe that, following a main avalanche A^* (identified by blue arrows in the right panel of Figure 4A), the sizes of activity cascades tend to rapidly decrease, with fluctuations that also decrease with the time elapsed from A^*. We refer to the activity following a main avalanche as the Omori sequence (Figure 4A, left panel), in analogy with the sequence of aftershocks that follows a main earthquake.

Such dynamics follow the attenuation-amplification principle over timescales ranging between a few seconds and a few tens of seconds and are strongly reminiscent of alpha "waxing and waning."[20] Following this analogy, we analyze the brain activity around the main avalanches A^*s. In Figure 4A (right), we show the analysis of a raster plot segment from an Omori sequence (marked in magenta in the left panel). We observe that the main avalanche identified in the raster plot (top) corresponds to higher amplitude alpha bursts (center), with large peaks in the alpha power $S(\alpha)$ (bottom). Furthermore, we notice that, before and after the main avalanche, the signal amplitude and the alpha power decrease considerably (Figure 4A, center and bottom).

Next, we proceed to quantify the Omori sequences by analyzing the number $N(t)$ of avalanches per unit time occurring after a time t has elapsed from the main avalanches. We find that $N(t)$ decays as t^{-p} across a wide range of ts in 4-min MEG and EEG recordings (Figure 4B). We observe that the exponent p is close to one for a range of threshold values s^* used to identify the main avalanches, and its value decreases when the threshold s^* becomes too large (Figure 4B, insets). This behavior is also observed in 40-min MEG recordings and is consistent across subjects (Figure S9). The power-law decay $N(t) \propto t^{-p}$ of the number of events following a main avalanche is consistent with the

CellPress
OPEN ACCESS

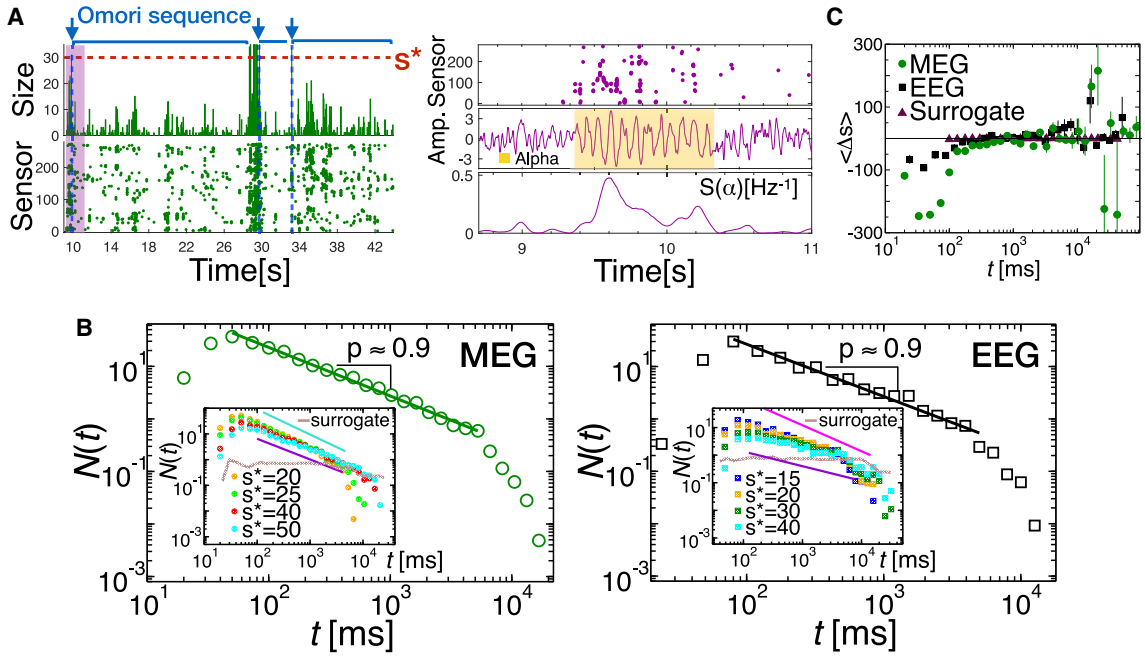

Figure 4. Alpha "waxing and waning" is described by the Omori law in the underlying neural cascading process

(A) A raster plot of 35 s of activity (left, bottom) and the corresponding avalanche sizes (left, top) showing three Omori sequences of different durations ranging between about 2 and 15 s and including several alpha cycles. Each sequence starts with a main avalanche A^* with a size larger than 30 (blue arrow). Activity decreases over time until the next main avalanche. The raster plot corresponding to the start of the first Omori sequence (highlighted in magenta in the left, bottom panel) is shown in the right, top panel. Brain activity around the main avalanche corresponds to high-amplitude alpha bursts (right, center; yellow shaded area), preceded and followed by lower-amplitude fluctuations. The instantaneous power at 10 Hz peaks around the main avalanche and then rapidly decreases (right, bottom).

(B) $N(t)$ as a function of the time t elapsed after a main avalanche A^* in 4-min MEG resting brain activity (left, individual subject). $N(t)$ decreases as the reciprocal of the time elapsed from the main avalanche A^*; i.e., $N(t) \propto t^{-p}$ with $p \simeq 1$ ($p = 0.9240 \pm 0.0169$. $s^* = 30$; $s^*/(\#MEGsensors) \simeq 0.11$). Inset: $N(t)$ for different values of the threshold s^* defining a main avalanche A^*. The exponent p ranges between 0.9773 ± 0.0302 (turquoise line) and 0.8054 ± 0.020 (violet line). Similar results are obtained in 40-min MEG recordings (Figure S9). The Omori law is also verified in the EEG of the resting state (right, individual subject), with $p = 0.9384 \pm 0.0321$ for $s^* = 10$ ($s^*/(\#EEGsensors) \simeq 0.16$). Power-law fits were performed using a maximum likelihood estimator and compared with exponential fits via log likelihood ratios (STAR Methods)[44] (MEG 4-min: $R = 270$, $p = 4 \cdot 10^{-17}$. EEG: $= 70$, $p = 3 \cdot 10^{-5}$). The p value measures the significance of R and is defined in the STAR Methods. In all cases, the power law is more likely to describe the empirical data. Inset: $N(t)$ for different values of the threshold s^* defining a main avalanche A^*. The exponent p describing the power-law decay of $N(t)$ ranges between 0.9384 ± 0.0321 (magenta line) and 0.5289 ± 0.0471 (violet line). $N(t)$ is independent of t in the surrogate data (insets, brown curves).

(C) Average $\Delta s = s_{i+1} - s_i$ between consecutive avalanches occurring within two main avalanches as a function of the time t elapsed from the first main avalanche (4-min MEG, n = 70; EEG, n = 6). Error bars represent the standard error of the mean. We note that, for surrogate data, Δs is independent of t and always close to zero (brown triangles).

generalized Omori law, $N(t) \propto (t+c)^{-p}$ (where c is a parameter related to onset of the power-law), which describes the temporal organization of aftershocks following a main earthquake.[50,51] The presence of the Omori law indicates that, after a main avalanche, the occurrence of the following avalanches is correlated over a wide range of timescales—up to several seconds, the location of the power-law cutoff. In particular, the power-law decay, $N(t) \propto t^{-1}$, implies that the activity after a large cascade is characterized by temporal clustering over unusually long timescales—up to tens of seconds—and that the alternation between high- and low-amplitude fluctuations does not have characteristic temporal scales.[18] In analogy with the earthquake dynamics, the Omori law for avalanches may be related to the slow build up and discharge of synaptic resource across neural populations following main avalanches.

Importantly, we observe that, within an Omori sequence, the average Δs between consecutive avalanches is always negative for $t < 100$ ms (Figure 4C). For t longer than a few hundreds of milliseconds, the average Δs tends to transitions to positive values, although larger statistical samples would be needed to make a robust assessment of $\langle \Delta s \rangle$ in this region.

Neural activity cascades during sleep do not obey AADs

We demonstrated that collective neural activity during resting wakefulness is characterized by AAD; namely, alternation of two distinct dynamical regimes: an attenuation regime within the alpha cycle and an amplification regime between alpha cycles (Figure 3). The AAD is part of the Omori-type dynamics encompassing resting-state brain activity over timescales of several seconds. To verify that these characteristics of the cascading dynamics are specific to the awake resting state dominated by the alpha rhythm, we next investigate the dynamics of neural cascades during NREM sleep. In contrast to the awake resting state, brain activity during NREM sleep shows

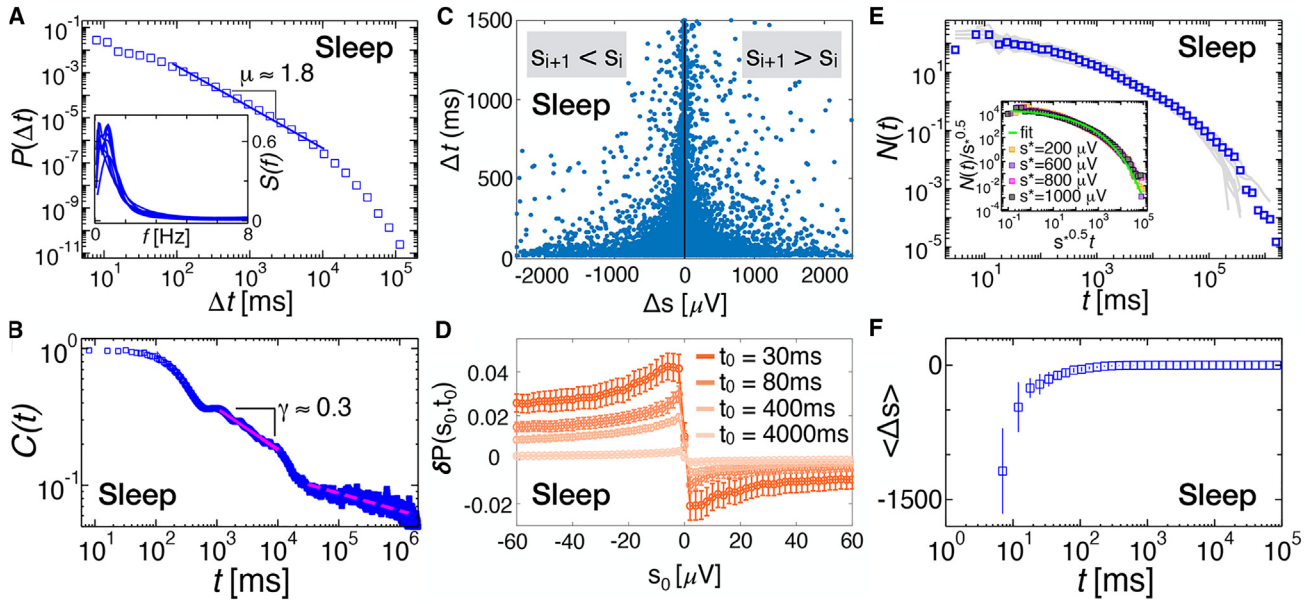

Figure 5. Neural activity cascades during sleep do not exhibit AAD and do not obey the Omori law

(A) Distributions of quiet times between consecutive avalanches during sleep (pooled data, n = 10). Unlike the resting state, during sleep, quiet-time distributions show a single power-law regime characterized by an exponent $\mu = 1.8311 \pm 0.0018$ ($R = 107$; STAR Methods) and followed by an exponential cutoff. Inset: power spectra for individual subjects. The maximum is always in the range of 0.5–2 Hz, within the delta band.

(B) Autocorrelation $C(t)$ of the instantaneous activity measured in each time bin ϵ. For $t < 500$ ms, $C(t)$ exhibits an exponential decay, which is followed by a plateau between 500 and 1,000 ms, corresponding to 1- 2 Hz delta oscillations. For $10^3 < t < 10^4$ ms, $C(t)$ decays as a power law with an exponent $\gamma = 0.3017 \pm 0.0011$.

(C) Scatter plot between Δs and Δt during sleep (all subjects). Negative Δss are positively correlated with their corresponding quiet times, whereas positive Δss are anti-correlated with their relative quiet times. The Spearman's correlation coefficient is positive for $\Delta s < 0$ and negative for $\Delta s > 0$: $\rho(\Delta s < 0, \Delta t) = 0.1627 \pm 0.0032$; $\rho(\Delta s > 0, \Delta t) = -0.1022 \pm 0.0041$.

(D) The quantity $\delta P(s_0, t_0)$ as a function of s_0 for different values of the threshold t_0 on Δts. The error bar on each data point is $2\sigma^*$ (σ^* is the SD associated with the surrogates P^*; STAR Methods). For each value of t_0, δP is always positive for $s_0 < 0$ and negative for $s_0 > 0$ and takes its maximum (minimum) at $s_0 \simeq -10$ ($s_0 \simeq 10$). Hence, for successive avalanches, the following avalanche tends to be smaller than the preceding one (attenuation regime), independently of the quiet time that separates them (cf. Figure 3).

(E) Number of avalanches per unit time, $N(t)$, occurring after a main avalanche A* (gray lines, individual subjects; symbols, pooled data). Unlike resting wakefulness, $N(t)$ does not obey the Omori law, but is well fitted by a stretched exponential $N(t) \propto e^{-(t/\tau)^\beta}$. Inset: $N(t)$ for different values of the threshold s^* used to define a main avalanche. Data for different s^*'s collapse onto a single curve when t is rescaled by $s^{*0.5}$. Green line, stretched exponential fit $N(t) \propto e^{-(t/\tau)^\beta}$, with $\beta = 0.25$.

(F) The average $\Delta s = s_{i+1} - s_i$ between consecutive avalanches occurring within two main avalanches is always negative and monotonically increases with t, the time elapsed from the main avalanche. Error bars represent the standard error of the mean.

a limited amount of alpha oscillations and instead is largely dominated by slow oscillations in the delta band (1–4 Hz).[4]

We consider EEG recordings across approximately 8 h of night sleep (STAR Methods) and analyze the distribution of quiet times between consecutive avalanches. We observe that, unlike the awake resting state, the distribution of quiet times during NREM sleep exhibits a single power-law regime with an exponent $\mu_s \simeq 1.8$, followed by an exponential decay for $\Delta t > 10$ s (Figure 5A). Correspondingly, the autocorrelation function $C(t)$ of the instantaneous activity, defined as the sum of the absolute values of all signals exceeding the threshold in a time bin, shows a power-law decay with an exponent $\gamma \simeq 0.3$ for 1 s $< t <$ 10 s, followed by a slower decay for larger ts (Figure 5B). Unlike in the awake resting state (Figure 2), during NREM sleep, $C(t)$ exhibits an exponential decay at shorter timescales ($t < 500ms$) (Figure 5B).

Next, we examine the scatter plot between the Δss and the corresponding Δts (Figure 5C). We find that large negative Δss occur with short quiet-time Δts, while positive size increments tend to be anti-correlated with the corresponding quiet times (Figure 5C). This behavior is similar to the behavior we observed during resting wakefulness (Figures 2E and 2F). However, the relationship between consecutive avalanches as a function of the time separation exhibits a rather different behavior during NREM sleep. We analyze the quantity $\delta P(s_0; t_0)$ defined in Figure 3 as a function of s_0 for a range of t_0 values between 30 and 4,000 ms (Figure 5D). We find that $\delta P(s_0; t_0)$ follows the attenuation regime defined in Figure 3 for all t_0 values (Figure 5D); namely, the size increments Δs between consecutive avalanches tend to be always negative. This implies that avalanche sizes preferentially exhibit a decreasing trend, an attenuation effect that is particularly strong for Δts shorter than 400 ms. Such a behavior is in stark contrast with our observations during resting wakefulness, where we found a transition from an attenuation regime—$\Delta s < 0$ for $\Delta t < 100$ ms—to an amplification regime—$\Delta s > 0$ for $\Delta t > 100$ ms—at the characteristic time of the alpha rhythm (Figure 3).

CellPress
OPEN ACCESS

We next analyze the number $N(t)$ of avalanches per unit time occurring after a time t has elapsed from a main avalanche A^*. We find that, unlike in the awake resting state, $N(t)$ decays according to a stretched exponential; that is, $N(t) \propto e^{-(t/\tau)^{\beta}}$ with $\beta = 0.25$. This behavior is consistent across subjects (Figure 5E, gray curves) and does not depend on the threshold s^* used to define the main avalanches A^*, as demonstrated by the data collapse in the inset of Figure 5E. Furthermore, in contrast to the awake resting state, we find that the average Δs in the sequence of avalanches between two main shocks is always negative and slowly approaches zero for $t > (1-2$ s) (Figure 5F).

DISCUSSION

In this paper, we provided a description of resting-state brain activity that uncovers the dynamic organization of neural activity cascades in relation to brain rhythms and offers new insights into the functional role of alpha oscillations in the awake resting state. Our analysis shows that the collective neural dynamics underlying resting-state brain activity is characterized by the rhythmic alternation of attenuation-amplification bouts, which is modulated by the alpha rhythm across multiple timescales. On a timescale of a few alpha cycles (< 1 s), attenuation of neural activity cascades is found within the typical length of the alpha cycle (i.e., about 100 ms),[1,2] while amplification of neural activity cascades occurs over timescales of a few hundreds of milliseconds. Significantly, the attenuation-to-amplification transition consistently correlates with the dominant frequency in the alpha band. We have shown that these short-term AADs are part of a large-scale, size-dependent temporal structure of neural cascades that obeys the Omori law[50]: large avalanches (main avalanches) are followed by increasingly smaller avalanches at a rate that decays as a power law of the time elapsed from the main avalanche—long-term AADs regulating brain activity over a timescale of seconds. Importantly, the short-term AADs and the Omori law are unique to the awake resting state and are not present during NREM sleep.

The dynamic structure of neural cascades during the awake resting state contains the hallmarks of two key functional characteristics of the alpha rhythm: (1) the timing of inhibition and excitation in cortical networks and (2) the fluctuations in amplitude known as "waxing and waning."[6,18–20,42,57,58] The short-term AAD reported in the present study indicates that inhibition may be activated to gradually suppress the cascading process within about 100 ms during the attenuation regime, while excitability is successively enhanced to amplify neural cascades over the timescales of a few alpha cycles (a few hundreds of milliseconds). Coherently, at the crossover between attenuation and amplification (i.e., at about the 100 ms characteristic of alpha waves), there is no clear monotonic relation between consecutive avalanches, which is consistent with a random organization of avalanche sizes—a clear transition signature. This is consistent with the hypothesis that alpha-mediated inhibition is applied in rhythmic cycles, a mechanism referred to as "pulsed inhibition."[8,30,31] At the same time, our findings also indicate an active role of alpha waves in timing the increase in network excitability (increased excitation or disinhibition), an effect not described previously. This suggests a dual role of alpha oscillations, going beyond the pulsed inhibition hypothesis. Furthermore, our analysis shows that the attenuation-amplification principle governs resting-state brain activity across scales, revealing a precise structure in the cascading process underlying the long-term "waxing and waning" phenomenon.[20] We found that the high-amplitude alpha bursts function as main inhibitory events. Between such events, which we call main avalanches, smaller and increasingly sparser cascades occur, obeying the short-term AADs. These observations indicate that the precise short-term dual role—attenuating and amplifying—of the alpha rhythm is embedded in a size-time dependent long-term organization captured by the Omori law. In contrast with the description of the waxing and waning as a multi-periodic phenomenon,[20] the range of variability implied by the power-law behavior of the Omori law indicates that the fluctuations associated with the "waxing and waning" of the alpha rhythm do not have a characteristic time, as recent studies have also suggested.[18,26] This may provide the brain with the flexibility necessary to organize complex streams of information while maintaining precise information control through timely short-term AADs.

Such findings point to an intermittent rather than periodic nature of alpha waxing and waning. This is in line with recent analyses of resting-state brain activity[18,26] showing that the power in the alpha band follows a bistable distribution, with large-scale high- and low-power modes. The dwell time in high- and low-power modes is distributed according to a stretched exponential, indicating that the alternation between modes is bursty, or erratic, in nature rather than periodic. We notice that, unlike neuronal avalanches, spatiotemporal events unfolding over multiple sensors across multiple time bins, these quantities are defined on single-sensor signals. Moreover, avalanches are a collective measure, and, as such, their dynamics arise from the complex relationship among all sensor signals (i.e., large and distinct populations of neurons). However, the building blocks of neuronal avalanches (i.e., excursions over threshold in individual signals) obey Weibull-like statistics,[23] indicating that, when constrained to the individual sensors signals that participate in the avalanches, there are close analogies with the results in Freyer et al.[18]

In stark contrast with our observations in the awake resting state, we found that the cascading process during NREM sleep, where the alpha rhythm is nearly absent, does not show AADs, and the avalanche occurrence rate after a large avalanche follows a stretched exponential decay. The stretched exponential can be understood as a superposition of exponential decays with different characteristic times. In this case, the cascading process can be seen as the superposition of many independently acting entities, each with a specific fixed cascading rate. Thus, the presence of a stretched exponential decay during sleep suggests that the corresponding emergent cortical patterns may depend on the complex interplay of the multiple brain regions controlling sleep regulation and on the coupling of different brain rhythms.[59–66] This further confirms that the AADs and the Omori law are related to the alpha rhythm dominating the awake resting state and suggests distinct generative mechanisms for the cascading process during NREM sleep. Despite the difference in avalanche dynamics between sleep and awake resting state reported here, neuronal avalanches

during sleep show power-law size and duration distributions consistent with criticality,[67,68] as observed in the awake resting state.[36,37]

We have shown that the distribution of quiet times between consecutive neural cascades, $P(\Delta t)$, exhibits two distinct power-law regimes and related this behavior to the presence of dominant alpha oscillations. The quiet time distribution has been investigated previously in other systems without alpha oscillations, and its behavior conditioned to the minimum avalanche size (i.e., $P(\Delta t|s > s_c)$, with s the avalanche size and s_c a threshold value) has also been studied.[35,39,49] In cortex slice cultures with up and down states and nested theta-gamma oscillations, $P(\Delta t)$ was found to follow a non-monotonic behavior with a power law followed by a hump and a faster decay, with the hump being located at the characteristic time of the slow up/down-state oscillations.[39,40,52] Furthermore, it was shown that, because of the presence of up- and down-states, the conditional distributions $P(\Delta t|s > s_c)$ do not collapse onto a unique scaling function when quiet times are rescaled by the mean quiet time, $\langle \Delta t \rangle$. Most importantly, and in line with our findings, $P(\Delta t|s > s_c)$ at the characteristic time of the theta oscillations (200 ms) has been found to be independent of s_c[39]. On the other hand, in freely behaving rats, a double power-law scaling function has been found to describe the $P(\Delta t|s > s_c)$ for a range of s_c.[35] In contrast with these findings and ours (Figures S4 and S5), the same analysis in zebrafish, where no oscillations are present, has shown that the quiet-time distributions for different thresholds s_c collapse onto a unique scaling function that is well described by a gamma distribution.[49] Overall, these observations indicate that the presence of prominent neural oscillations is connected with non-homogeneous forms of the quiet-time distribution as well as a peculiar relationship between Δt and avalanche sizes s, where the transition between distinct scaling behaviors coincides with the characteristic period of the dominant oscillations.

Our analysis of neural activity cascades in relation to brain rhythms lays the basis for a unifying view of two complementary approaches to neural synchronization: neuronal avalanches and oscillations. On one hand, brain rhythms have characteristic times and amplitudes and are, by definition, a property of the integrated electromagnetic signals arising from the superposition of synaptic currents from large neural populations. On the other hand, neuronal avalanches exhibit scale-free, power-law statistical properties and show a consistent spatiotemporal organization in terms of discrete events, from sequences of spiking neurons[49,69–72] to clusters of extreme amplitude fluctuations in local field potentials (LFP), EEG, and MEG sensor arrays.[33,34,36,37] The coexistence of neuronal avalanches and oscillations has been investigated previously in mature cortex slice cultures, rodents, and non-human primates, where nested theta and beta/gamma oscillations embedded in avalanches have been reported,[38,39,41] and a hierarchical organization of theta and gamma oscillations was identified.[39] In line with our observations pointing to substantial differences between cascading processes during distinct physiological states (i.e., awake resting state and NREM sleep), studies of spontaneous activity in mature cortex slice cultures showed that avalanche dynamics are highly sensitive to the excitation-inhibition balance.[52–54] Furthermore, a temporal structure of neuronal avalanches consistent with the Omori law was also identified by Plenz.[55] Recently, the relation between neuronal avalanches, gamma oscillations, and emergent signatures of critical dynamics has been studied in non-human primates.[41] On the other hand, in the human brain, the relationship between avalanche dynamics and oscillations had not been scrutinized to date. Indeed, simultaneous investigations of oscillations and avalanches in the human brain selectively focused on LRTCs in alpha amplitude fluctuations and on avalanche scaling features.[17,73] At the same time, models showing simultaneous emergence of avalanches and oscillatory behaviors mostly concentrated on underlying mechanisms or signatures of criticality.[22,23,74–77] In particular, a quantitative analysis of awake resting-state brain activity through a class of adaptive neural networks recently linked the coexistence of alpha oscillations and avalanches to proximity to a non-equilibrium critical point at the onset of self-sustained oscillations.[23,78] In this context, the present study establishes the first functional and dynamic links between neural oscillations and avalanches in the awake resting state, uncovering a deep relationship between two collective phenomena with antithetic features: scale-free avalanches and scale-specific brain rhythms.

Overall, the analysis of accessible, near-synchronous collective behaviors shows that the alpha rhythm functions as a pacemaker for network excitability during the awake resting state. The AADs identified here correlate with alpha rhythmicity and shape neural activity on multiple timescales, from a few hundreds of milliseconds to several seconds, indicating that alpha regulates the timing of inhibition and excitation bouts in the awake resting-state brain activity. The results suggest a unifying view of the pulsed inhibition function and the "waxing and waning" phenomenon, where the latter is a mechanism that regulates long-term, resting wakefulness network excitability. Future work will focus on the role of AADs in information processing. In this respect, the approach we put forward will allow us to (1) directly verify, and potentially extend, the pulsed inhibition hypothesis[8,30] through analysis of the AADs in relation to processing of sensory stimuli and (2) clarify the functional role of the "waxing and waning" phenomena. More generally, our approach outlines a coherent view of the dichotomy of scale-specific oscillations and scale-free avalanches[23,38,39,41,54] and demonstrates a functional and informative connection between these two phenomena. This may prove useful to dissect collective neural dynamics underlying brain oscillations in contexts where simultaneous recordings of single-cells and coarse-grained signals are out of reach, harvesting information from the analysis of neural cascading processes that would not be accessible otherwise.

Limitations of the study

We identified hallmarks of alpha-mediated pulses of attenuation and amplification of neural activity cascades from MEG and EEG recordings. However, simultaneous multiscale recordings will be needed to relate the reported large-scale dynamics with the collective behavior of a local neural population, in particular modulation of inhibitory versus excitatory neural population activity. This is a key step toward assessing whether alpha oscillations drive alternating pulses of inhibition and excitation, as our results

CellPress
OPEN ACCESS

seem to indicate. To further validate the link between AADs and alpha rhythm, a future analysis of the alpha-depressed resting state is needed to be also compared with the reported evidence of AAD absence during NREM sleep.

In addition, we note that the alpha rhythm is also present during REM sleep.[4,79] However, here, we limited our investigation to the functional role of alpha oscillations in resting wakefulness because we were interested in finding evidence of alpha-mediated pulsed inhibition.[30] The presence of AADs in relation to alpha oscillations during REM sleep should be of great interest for future work.

STAR★METHODS

Detailed methods are provided in the online version of this paper and include the following:

- KEY RESOURCES TABLE
- RESOURCE AVAILABILITY
  - Lead contact
  - Materials availability
  - Data and code availability
- EXPERIMENTAL MODEL AND STUDY PARTICIPANT DETAILS
  - MEG of the eyes-closed awake resting state
  - EEG of the eyes-closed awake resting state
  - Sleep EEG
- METHOD DETAILS
  - Data acquisition and pre-processing
  - Analysis of collective neural activity
- QUANTIFICATION AND STATISTICAL ANALYSIS

SUPPLEMENTAL INFORMATION

Supplemental information can be found online at https://doi.org/10.1016/j.celrep.2023.113162.

ACKNOWLEDGMENTS

This research was funded in whole or in part by the Austrian Science Fund (FWF) (grant PT1013M03318 to F.L.). For the purpose of open access, the author has applied a CC BY public copyright license to any Author Accepted Manuscript version arising from this submission. The study was supported by the European Union Horizon 2020 Research and Innovation Program under the Marie Sklodowska-Curie action (grant agreement 754411 to F.L.) and in part by the NextGenerationEU through the grant TAlent in ReSearch@University of Padua – STARS@UNIPD (to F.L.) (project BRAINCIP [brain criticality and information processing]). L.d.A. acknowledges support from the Italian MIUR project PRIN2017WZFTZP and partial support from NEXTGENERATIONEU (NGEU) funded by the Ministry of University and Research (MUR), National Recovery and Resilience Plan (NRRP), and project MNESYS (PE0000006)—a multiscale integrated approach to the study of the nervous system in health and disease (DN. 1553 11.10.2022). O.S. acknowledges support from the Israel Science Foundation, grant 504/17. The work was supported in part by DIRP ZIAMH02797 (to D.P.).

AUTHOR CONTRIBUTIONS

Conceptualization, F.L., L.d.A., and O.S.; methodology, F.L., L.d.A., and O.S.; formal analysis, F.L. and S.S.; investigation, all authors; writing – original draft, F.L.; writing – review & editing, all authors; visualization, F.L.

DECLARATION OF INTERESTS

The authors declare no competing interests.

INCLUSION AND DIVERSITY

We support inclusive, diverse, and equitable conduct of research.

Received: May 16, 2022
Revised: June 7, 2023
Accepted: September 7, 2023

REFERENCES

1. Buzsaki, G., and Draguhn, A. (2004). Neuronal oscillations in cortical networks. Science *304*, 1926–1929.
2. Berger, H. (1929). Ueber das Elektroenkephalogram des Menschen. Arch. Psychiatr. Nervenkr. *87*, 527–570.
3. Buzsáki, G., and Watson, B.O. (2012). Brain rhythms and neural syntax: implications for efficient coding of cognitive content and neuropsychiatric disease. Dialogues Clin. Neurosci. *14*, 345–367.
4. Rechtschaffen, K.A. (1968). A Manual of Standardized Terminology, Techniques and Scoring System for Sleep Stages of Human Subjects (U.S. Dept. of Health, Education, and Welfare).
5. Bashan, A., Bartsch, R.P., Kantelhardt, J.W., Havlin, S., and Ivanov, P.C. (2012). Network physiology reveals relations between network topology and physiological function. Nat. Commun. *3*, 702.
6. Pfurtscheller, G., Stancák, A., Jr., and Neuper, C. (1996). Event-related synchronization (ers) in the alpha band – an electrophysiological correlate of cortical idling: a review. Int. J. Psychophysiol. *24*, 39–46.
7. Pfurtscheller, G. (1992). Event-related synchronization (ers): an electrophysiological correlate of cortical areas at rest. Electroencephalogr. Clin. Neurophysiol. *83*, 62–69.
8. Mathewson, K.E., Lleras, A., Beck, D.M., Fabiani, M., Ro, T., and Gratton, G. (2011). Pulsed out of awareness: EEG alpha oscillations represent a pulsed-inhibition of ongoing cortical processing. Front. Psychol. *2*, 99.
9. Brickwedde, M., Krüger, M.C., and Dinse, H.R. (2019). Somatosensory alpha oscillations gate perceptual learning efficiency. Nat. Commun. *10*, 263.
10. Saalmann, Y.B., Pinsk, M.A., Wang, L., Li, X., and Kastner, S. (2012). The pulvinar regulates information transmission between cortical areas based on attention demands. Science *337*, 753–756.
11. Samaha, J., Sprague, T.C., and Postle, B.R. (2016). Decoding and reconstructing the focus of spatial attention from the topography of alpha-band oscillations. J. Cognit. Neurosci. *28*, 1090–1097.
12. Sadaghiani, S., and Kleinschmidt, A. (2016). Brain networks and α-oscillations: structural and functional foundations of cognitive control. Trends Cognit. Sci. *20*, 805–817.
13. Chapeton, J.I., Haque, R., Wittig, J.H., Jr., Inati, S.K., and Zaghloul, K.A. (2019). Large-scale communication in the human brain is rhythmically modulated through alpha coherence. Curr. Biol. *29*, 2801–2811.e5.
14. Becker, R., Knock, S., Ritter, P., and Jirsa, V. (2015). Relating alpha power and phase to population firing and hemodynamic activity using a thalamocortical neural mass model. PLoS Comput. Biol. *11*, e1004352.
15. Haegens, S., Nácher, V., Luna, R., Romo, R., and Jensen, O. (2011). α-oscillations in the monkey sensorimotor network influence discrimination performance by rhythmical inhibition of neuronal spiking. Proc. Natl. Acad. Sci. USA *108*, 19377–19382.
16. Linkenkaer-Hansen, K., Nikouline, V.V., Palva, J.M., and Ilmoniemi, R.J. (2001). Long-range temporal correlations and scaling behavior in human brain oscillations. J. Neurosci. *21*, 1370–1377.

17. Palva, J.M., Zhigalov, A., Hirvonen, J., Korhonen, O., Linkenkaer-Hansen, K., and Palva, S. (2013). Neuronal long-range temporal correlations and avalanche dynamics are correlated with behavioral scaling laws. Proc. Natl. Acad. Sci. USA *110*, 3585–3590.
18. Freyer, F., Aquino, K., Robinson, P.A., Ritter, P., and Breakspear, M. (2009). Bistability and non-gaussian fluctuations in spontaneous cortical activity. J. Neurosci. *29*, 8512–8524.
19. Motokawa, K. (1942). Die Analyse der Perioden im normalen Elektroencephalogramm des Menschen. Tohoku J. Exp. Med. *42*, 9–20.
20. Mimura, K. (1971). On the periodic fluctuations of alpha waves. Jpn. J. Physiol. *21*, 375–386.
21. Wang, X.-J. (2010). Neurophysiological and computational principles of cortical rhythms in cognition. Phys. Rev. *90*, 1195–1268.
22. Poil, S.-S., Hardstone, R., Mansvelder, H.D., and Linkenkaer-Hansen, K. (2012). Critical-state dynamics of avalanches and oscillations jointly emerge from balanced excitation/inhibition in neuronal networks. J. Neurosci. *32*, 9817–9823.
23. Lombardi, F., Pepić, S., Shriki, O., Tkačik, G., and De Martino, D. (2023). Statistical modeling of adaptive neural networks explains co-existence of avalanches and oscillations in resting human brain. Nat. Comput. Sci. *3*, 254–263. https://doi.org/10.1038/s43588-023-00410-9.
24. Vijayan, S., and Kopell, N.J. (2012). Thalamic model of awake alpha oscillations and implications for stimulus processing. Proc. Natl. Acad. Sci. USA *109*, 18553–18558.
25. Vijayan, S., Ching, S., Purdon, P.L., Brown, E.N., and Kopell, N.J. (2013). Thalamocortical mechanisms for the anteriorization of alpha rhythms during propofol-induced unconsciousness. J. Neurosci. *33*, 11070–11075.
26. Freyer, F., Roberts, J.A., Becker, R., Robinson, P.A., Ritter, P., and Breakspear, M. (2011). Biophysical mechanisms of multistability in resting-state cortical rhythms. J. Neurosci. *31*, 6353–6361.
27. Deco, G., Kringelbach, M.L., Jirsa, V.K., and Ritter, P. (2017). The dynamics of resting fluctuations in the brain: metastability and its dynamical cortical core. Sci. Rep. *7*, 3095.
28. Halász, P., Terzano, M., Parrino, L., and Bódizs, R. (2004). The nature of arousal in sleep. J. Sleep Res. *13*, 1–23.
29. Parrino, L., Ferri, R., Bruni, O., and Terzano, M.G. (2012). Cyclic alternating pattern (cap): The marker of sleep instability. Sleep Med. Rev. *16*, 27–45.
30. Klimesch, W., Sauseng, P., and Hanslmayr, S. (2007). Eeg alpha oscillations: The inhibition–timing hypothesis. Brain Res. Rev. *53*, 63–88.
31. Mazaheri, A., and Jensen, O. (2010). Rhythmic pulsing: linking ongoing brain activity with evoked responses. Front. Hum. Neurosci. *4*, 177.
32. Klimesch, W. (2012). α-band oscillations, attention, and controlled access to stored information. Trends Cognit. Sci. *16*, 606–617.
33. Beggs, J.M., and Plenz, D. (2003). Neuronal avalanches in neocortical circuits. J. Neurosci. *23*, 11167–11177.
34. Petermann, T., Thiagarajan, T.C., Lebedev, M.A., Nicolelis, M.A.L., Chialvo, D.R., and Plenz, D. (2009). Spontaneous cortical activity in awake monkeys composed of neuronal avalanches. Proc. Natl. Acad. Sci. USA *106*, 15921–15926.
35. Ribeiro, T.L., Copelli, M., Caixeta, F., Belchior, H., Chialvo, D.R., Nicolelis, M.A.L., and Ribeiro, S. (2010). Spike avalanches exhibit universal dynamics across the sleep-wake cycle. PLoS One *5*, e14129.
36. Shriki, O., Alstott, J., Carver, F., Holroyd, T., Henson, R.N.A., Smith, M.L., Coppola, R., Bullmore, E., and Plenz, D. (2013). Neuronal avalanches in the resting meg of the human brain. J. Neurosci. *33*, 7079–7090.
37. Lombardi, F., Shriki, O., Herrmann, H.J., and de Arcangelis, L. (2021). Long-range temporal correlations in the broadband resting state activity of the human brain revealed by neuronal avalanches. Neurocomputing *461*, 657–666.
38. Gireesh, E.D., and Plenz, D. (2008). Neuronal avalanches organized as nested theta-and beta/gamma-oscillations during development of cortical layer 2/3. Proc. Natl. Acad. Sci. USA *105*, 7576–7581.
39. Lombardi, F., Herrmann, H.J., Plenz, D., and de Arcangelis, L. (2014). On the temporal organization of neuronal avalanches. Front. Syst. Neurosci. *8*, 204.
40. Lombardi, F., and de Arcangelis, L. (2014). Temporal organization of ongoing brain activity. Eur. Phys. J. Spec. Top. *223*, 2119–2130.
41. Miller, S.R., Yu, S., and Plenz, D. (2019). The scale-invariant, temporal profile of neuronal avalanches in relation to cortical γ–oscillations. Sci. Rep. *9*, 16403.
42. Walter, W.G. (1960). Intrinsic Rhythms of the Brain, D.C. Washington, ed. (Neurophysiology: Amer. Physiol. Soc.), pp. 279–298. Ch. Section 1.
43. Tagliazucchi, E., Balenzuela, P., Fraiman, D., and Chialvo, D.R. (2012). Criticality in large-scale brain fmri dynamics unveiled by a novel point process analysis. Front. Physiol. *3*, 15.
44. Alstott, J., Bullmore, E., and Plenz, D. (2014). powerlaw: A python package for analysis of heavy-tailed distributions. PLoS One *9*, e85777.
45. Marshall, N., Timme, N.M., Bennett, N., Ripp, M., Lautzenhiser, E., and Beggs, J.M. (2016). Analysis of Power Laws, Shape Collapses, and Neural Complexity: New Techniques and MATLAB Support via the NCC Toolbox. Front. Physiol. *7*, 250. https://doi.org/10.3389/fphys.2016.00250.
46. Buldyrev, S.V. (2009). Fractals in Biology. In Encyclopedia of Complexity and System Science, Robert A. Meyers, ed. (New York: Springer), pp. 3779–3802.
47. Rybski, D., Buldyrev, S.V., Havlin, S., Liljeros, F., and Makse, H.A. (2009). Scaling laws of human interaction activity. Proc.Natl.Acad.Sci.USA *106*, 12640–12645.
48. Rybski, D., Buldyrev, S.V., Havlin, S., Liljeros, F., and Makse, H.A. (2012). Communication activity in a social network: relation between long-term correlations and inter-event clustering. Sci. Rep. *2*, 560.
49. Ponce-Alvarez, A., Jouary, A., Privat, M., Deco, G., and Sumbre, G. (2018). Whole-brain neuronal activity displays crackling noise dynamics. Neuron *100*, 1446–1459.e6.
50. Utsu, T. (2002). International Handbook of Earthquake and Engineering Seismology, *81A* (Academic Press).
51. de Arcangelis, L., Godano, C., Grasso, J.R., and Lippiello, E. (2016). Statistical physics approach to earthquake occurrence and forecasting. Phys. Rep. *628*, 1–91.
52. Lombardi, F., Herrmann, H.J., Perrone-Capano, C., Plenz, D., and de Arcangelis, L. (2012). Balance between excitation and inhibition controls the temporal organization of neuronal avalanches. Phys. Rev. Lett. *108*, 228703.
53. Lombardi, F., Herrmann, H.J., Plenz, D., and de Arcangelis, L. (2016). Temporal correlations in avalanche occurrence. Sci. Rep. *6*, 24690.
54. Lombardi, F., Herrmann, H.J., and de Arcangelis, L. (2019). Avalanche Dynamics and Correlations in Neural Systems. In The Functional Role of Critical Dynamics in Neural Systems. Springer Series on Bio- and Neurosystems, vol 11, N. Tomen, J. Herrmann, and U. Ernst, eds. (Cham: Springer). https://doi.org/10.1007/978-3-030-20965-0_1.
55. Plenz, D. (2012). Neuronal avalanches and coherence potentials. Eur. Phys. J. Spec. Top. *205*, 259–301.
56. Corral, A. (2003). Local distributions and rate fluctuations in a unified scaling law for earthquakes. Phys. Rev. E *68*, 035102. (R).
57. Clayton, M.S., Yeung, N., and Cohen Kadosh, R. (2018). The many characters of visual alpha oscillations. Eur. J. Neurosci. *48*, 2498–2508.
58. Fries, P. (2005). A mechanism for cognitive dynamics: neuronal communication through neuronal coherence. Trends Cognit. Sci. *9*, 474–480.
59. Lakatos, P., Shah, A.S., Knuth, K.H., Ulbert, I., Karmos, G., and Schroeder, C.E. (2005). An oscillatory hierarchy controlling neuronal excitability and stimulus processing in the auditory cortex. J. Neurophysiol. *94*, 1904–1911.
60. Behn, C.G.D., Brown, E.N., Scammell, T.E., and Kopell, N.J. (2007). Mathematical model of network dynamics governing mouse sleep-wake behavior. J. Neurophysiol. *97*, 3828–3840. https://doi.org/10.1152/jn.01184.2006.
61. Roopun, A.K., Kramer, M.A., Carracedo, L.M., Kaiser, M., Davies, C.H., Traub, R.D., Kopell, N.J., and Whittington, M.A. (2008). Temporal

interactions between cortical rhythms. Front. Neurosci. *2*, 145–154. https://doi.org/10.3389/neuro.01.034.2008.

62. Saper, C.B., Fuller, P.M., Pedersen, N.P., Lu, J., and Scammell, T.E. (2010). Sleep state switching. Neuron *68*, 1023–1042. https://doi.org/10.1016/j.neuron.2010.11.032.
63. Lombardi, F., Gómez-Extremera, M., Bernaola-Galván, P., Vetrivelan, R., Saper, C.B., Scammell, T.E., and Ivanov, P.C. (2020). Critical dynamics and coupling in bursts of cortical rhythms indicate non-homeostatic mechanism for sleep-stage transitions and dual role of vlpo neurons in both sleep and wake. J. Neurosci. *40*, 171–190.
64. Wang, J.W.J.L., Lombardi, F., Zhang, X., Anaclet, C., and Ivanov, P.C. (2019). Non-equilibrium critical dynamics of bursts in θ and δ rhythms as fundamental characteristic of sleep and wake micro-architecture. PLoS Comput. Biol. *15*, e1007268.
65. Bartsch, R.P., Liu, K.K.L., Bashan, A., and Ivanov, P.C. (2015). Network physiology: How organ systems dynamically interact. PLoS One *10*, e0142143.
66. Lombardi, F., Wang, J.W.J.L., Zhang, X., and Ivanov, P.C. (2020). Power-law correlations and coupling of active and quiet states underlie a class of complex systems with self-organization at criticality. EPJ Web Conf. *230*, 00005.
67. Priesemann, V., Valderrama, M., Wibral, M., and Le Van Quyen, M. (2013). Neuronal avalanches differ from wakefulness to deep sleep–evidence from intracranial depth recordings in humans. PLoS Comput. Biol. *9*, e1002985.
68. Scarpetta, S., Morrisi, N., Mutti, C., Azzi, N., Trippi, I., Ciliento, R., Apicella, I., Messuti, G., Angiolelli, M., Lombardi, F., et al. (2023). Criticality of neuronal avalanches in human sleep and their relationship with sleep macro- and micro-architecture. iScience *26*, 107840. https://doi.org/10.1016/j.isci.2023.107840.
69. Pasquale, V., Massobrio, P., Bologna, L.L., Chiappalone, M., and Martinoia, S. (2008). Self-organization and neuronal avalanches in networks of dissociated cortical neurons. J. Neurosci. *153*, 1354–1369.
70. Mazzoni, A., Broccard, F.D., Garcia-Perez, E., Bonifazi, P., Ruaro, M.E., and Torre, V. (2007). On the dynamics of the spontaneous activity in neuronal networks. PLoS One *2*, e439.
71. Ma, Z., Turrigiano, G.G., Wessel, R., and Hengen, K.B. (2019). Cortical circuit dynamics are homeostatically tuned to criticality in vivo. Neuron *104*, 655–664.e4.
72. Fontenele, A.J., de Vasconcelos, N.A.P., Feliciano, T., Aguiar, L.A.A., Soares-Cunha, C., Coimbra, B., Dalla Porta, L., Ribeiro, S., Rodrigues, A.J., Sousa, N., et al. (2019). Criticality between cortical states. Phys. Rev. Lett. *122*, 208101.
73. Zhigalov, A., Arnulfo, G., Nobili, L., Palva, S., and Palva, J.M. (2015). Relationship of fast- and slow-timescale neuronal dynamics in human meg and seeg. J. Neurosci. *35*, 5385–5396.
74. Scarpetta, S., Giacco, F., Lombardi, F., and De Candia, A. (2013). Effects of poisson noise in a if model with stdp and spontaneous replay of periodic spatiotemporal patterns, in absence of cue stimulation. Biosystems *112*, 258–264.
75. Scarpetta, S., and De Candia, A. (2014). Alternation of up and down states at a dynamical phase-transition of a neural network with spatiotemporal attractors. Front. Syst. Neurosci. *8*, 88.
76. Di Santo, S., Villegas, P., Burioni, R., and Muñoz, M.A. (2018). Landau–Ginzburg theory of cortex dynamics: Scale-free avalanches emerge at the edge of synchronization. Proc. Natl. Acad. Sci. USA *115*, E1356–E1365.
77. Kinouchi, O., Brochini, L., Costa, A.A., Campos, J.G.F., and Copelli, M. (2019). Stochastic oscillations and dragon king avalanches in self-organized quasi-critical systems. Sci. Rep. *9*, 3874.
78. Lombardi, F., and De Martino, D. (2023). Oscillations and avalanches coexist in brain networks close to criticality. Nat Comput Sci *3*, 194–195. https://doi.org/10.1038/s43588-023-00411-8.
79. Cantero, J.L., Atienza, M., and Salas, R.M. (2002). Human alpha oscillations in wakefulness, drowsiness period, and rem sleep: different electroencephalographic phenomena within the alpha band. Neurophysiol. Clin. *32*, 54–71.
80. Yu, S., Yang, H., Shriki, O., and Plenz, D. (2013). Universal organization of resting brain activity at the thermodynamic critical point. Front. Syst. Neurosci. *7*, 42.
81. Delorme, A., and Makeig, S. (2004). Eeglab: an open source toolbox for analysis of single-trial eeg dynamics including independent component analysis. J. Neurosci. Methods *134*, 9–21.
82. Mullen, T.R., Kothe, C.A.E., Chi, Y.M., Ojeda, A., Kerth, T., Makeig, S., Jung, T.P., and Cauwenberghs, G. (2015). Real-time neuroimaging and cognitive monitoring using wearable dry eeg. IEEE Trans. Biomed. Eng. *62*, 2553–2567.
83. Bell, A.J., and Sejnowski, T.J. (1995). An information-maximization approach to blind separation and blind deconvolution. Neural Comput. *7*, 1129–1159.
84. Theiler, J., Eubank, S., Longtin, A., Galdrikian, B., and Doyne Farmer, J. (1992). Testing nonlinearity in time series: the method of surrogate data. Physica D *58*, 77–94.
85. Clauset, A., Shalizi, C.R., and Newman, M.E.J. (2009). Power-law distributions in empirical data. SIAM Rev. *51*, 661–703.

STAR★METHODS

KEY RESOURCES TABLE

REAGENT or RESOURCE	SOURCE	IDENTIFIER
Experimental models: Organisms/strains		
Humans (MEG)	(Shriki et al.)[36]	https://www.jneurosci.org/content/33/16/7079
Humans (EEG resting wake)	This paper	N/A
Humans (EEG sleep)	This paper	N/A
Software and algorithms		
MATLAB R2020b	Mathworks	www.mathworks.com
Python version 3.1	Python Software Foundation	www.python.org
powerlaw	(Alstott et al.)[46]	https://github.com/jeffalstott/powerlaw

RESOURCE AVAILABILITY

Lead contact

Further information and requests for resources and reagents should be directed to and will be fulfilled by the lead contact, Fabrizio Lombardi (fabrizio.lombardi@ist.ac.at).

Materials availability

This study did not generate new unique reagents.

Data and code availability

- This study did not generate any new datasets. Data reported in this paper will be shared by the lead contact upon request.
- This study does not report original code.
- Any additional information required to reanalyze the data reported in this paper is available from the lead contact upon request.

EXPERIMENTAL MODEL AND STUDY PARTICIPANT DETAILS

MEG of the eyes-closed awake resting state

This study uses datasets previously collected at the NIMH. The 4-min MEG data are the same as used in[36]. The 40-min data are the same as used in.[80] Ongoing brain activity was recorded from 100 healthy participants (38 males and 66 females; age, 31.8 ± 11.8 y) in the MEG core facility at the NIMH (Bethesda, MD, USA) for a duration of 4 min (eyes closed), and from three healthy female (age range 24–29) participants for a duration of 40 min (eyes closed). All experiments were carried out in accordance with NIH guidelines for human subjects. For the present studies 73 subjects [70 (4 min) + 3 (40 min)] with a dominant alpha peak and AAD transition were selected.

EEG of the eyes-closed awake resting state

Resting-state EEG was recorded for 3 min (eyes closed) from six right-handed healthy volunteers (age range 22–27). Participants had no history of neurological or psychiatric diseases and had normal or corrected-to-normal vision. All participants gave written informed consent, and were paid for their participation. The study was approved by a local ethics committee (Ben-Gurion University) and was in accordance with the ethical standards of the Declaration of Helsinki.

Sleep EEG

The data analyzed in this study were extracted from overnight polysomnography (PSG) recordings acquired at the Parma Sleep Disorders Center. Ten healthy subjects, 5 males and 5 females (age range 28–53 y; average age was 39,6 y) were selected after an entrance investigation based on the following inclusion criteria: (i) absence of any psychiatric, medical, and neurological disorders; (ii) normal sleep/wake habits without any difficulties in falling or remaining asleep at night. A personal interview integrated by a structured questionnaire confirmed good vigilance level during the daytime; and (III) no drug intake at the time of the PSG or the month before.

CellPress
OPEN ACCESS

METHOD DETAILS

Data acquisition and pre-processing

MEG of the eyes-closed awake resting state

The sampling rate was 600 Hz, and the data were band-pass filtered between 1 and 80 Hz. Power-line interferences were removed using a 60-Hz notch filter designed in MATLAB (Mathworks). The sensor array consisted of 275 axial first-order gradiometers. Two dysfunctional sensors were removed, leaving 273 sensors in the analysis. Analysis was performed directly on the axial gradiometer waveforms.

EEG of the eyes-closed awake resting state

EEG was recorded using the g.tec HIamp system (g.tec, Austria) with 64 gel-based electrodes (AgCl electrolyte gel). Electrodes were positioned according to the standard 10/20 system with linked ears reference. Impedances of all electrodes were kept below 5 k Ω. Data were pre-processed using a combination of the EEGLAB MATLAB toolbox[81] routines and custom code. After high-pass filtering (cut-off 1 Hz), a customized adaptive filter was applied to suppress line-noise. This was followed by Artifact Subspace Reconstruction,[82] re-referencing to the mean, and low-pass filtering (cutoff 60 Hz). Subsequently, an ICA (independent component analysis) algorithm was applied to the data.[83] The resulting ICs were evaluated automatically for artifacts by combining spatial, spectral and temporal analysis of ICs. ICs identified as containing ocular, muscular, or cardiac artifacts were removed from the data

Sleep EEG

Full-night unattended PSG recordings were performed with EOG (2 channels), EEG (19 channels in 7 subjects, Ag/AgCl electrodes placed according to the 10–20 International System referred to linked-ear lobes: Fp2, F4, C4, P4, O2, F8, T4, T6, Fz, Cz, Pz, Fp1, F3, C3, P3, O1, F7, T3, T5; 25 channels in 3 subjects: CP3, CP4, C5, C6, C2, C1, FC4, FC3, F4, C4, P4, O2, F8, T4, T6, Fz, Cz, Pz, F3, C3, P3, O1, F7, T3, T5), EMG of the submentalis muscle, ECG, body position monitor, and signal for SpO2 (pulse-oximetry O2-saturation). Sleep EEG recordings were obtained using a Brain Quick Micromed System 98 (Micromed, SPA) recording machine. The institutional Ethical Committee Area Vasta Emilia Nord approved the study (protocol no. 19750). Sleep was scored visually in 30-s epochs using standard criteria.[4]

Analysis of collective neural activity

MEG and EEG of the eyes-closed awake resting state

For each MEG (EEG) sensor, positive and negative deflections in the MEG (EEG) signal were detected by applying a threshold h at $\pm n$ SD. Comparison of the signal distribution to the best fit Gaussian indicates that the two distributions start to deviate from one another around 2.7SD.[36] Thus, thresholds smaller than 2.7SD will lead to the detection of many events related to noise in addition to real events, whereas much larger thresholds will miss many of the real events. To avoid noise-related events while preserving most of relevant events, in this study, we used threshold values $h > 2.9$ SD. To ensure a similar event rate across different sets of recordings (4-min MEG, 40-min MEG, 3-min EEG), we used the following h values: 3.3 SD for 4-min MEG; 3 SD for 40-min MEG, and 3 SD for 3-min EEG. In each excursion beyond the threshold, a single event was identified at the most extreme value (maximum for positive excursions and minimum for negative excursions). Data were binned using a time window $\epsilon = 2T_{meg} = 3.3$ ms and $\epsilon = T_{eeg} = 4$ ms for MEG and EEG data, respectively. $T_{meg} = 1.67$ ms was the sampling interval for MEG recordings, while $T_{eeg} = 4$ ms was the sampling interval for EEG recordings. A neural activity cascade, or avalanche, was defined as a continuous sequence of time bins in which there was at least one event on any sensor, ending with a time bin with no events on any sensor. The size of an avalanche, s, was defined as the number of events in the avalanche. For more details, see[36]. The size of an avalanche can be equivalently defined as the sum over all channels of the absolute values of the signals exceeding the threshold (Figure S10).

Sleep EEG

To identify avalanches during sleep, positive and negative deflections were detected by applying a threshold $h \pm 2$ SD (comparison of the signal distribution to the best fit Gaussian indicates that the two distributions start to deviate from one another at around 2SD). An avalanche was then defined as a continuous time interval in which there was at least one EEG channel supra-threshold. Due to the reduced number of electrodes in EEG sleep recordings, the size of an avalanche was defined as the sum over all channels of the absolute values of the signals exceeding the threshold. This definition is equivalent to the definition of avalanche size as the number of electrodes with positive (negative) deflections exceeding the threshold h[33] (Figure S10).

Conditional probabilities analysis

Each recording results in a sequence of avalanches a_i, and corresponding sizes s_i (Figure 1). The quantity $\Delta s = s_{i+1} - s_i$ is the difference between the sizes of two consecutive avalanches a_i and a_{i+1}, and is used to study their monotonic relation—i.e. whether s_i is more likely to be smaller or larger than s_{i+1}—as a function of the quiet times Δt occurring in between. To this end, the following conditional probability is defined,

$$P(\Delta s < s_0 \mid \Delta t < t_0) \equiv \frac{N(\Delta s < s_0, \Delta t < t_0)}{N(\Delta t < t_0)},$$

where $N(\Delta s < s_0, \Delta t < t_0)$ is the number of avalanche couples which are separated by a quiet time Δt shorter than a given t_0 and whose size difference Δs is smaller than a given s_0, and $N(\Delta t < t_0)$ is the number of quiet times Δt shorter than t_0. $P(\Delta s < s_0 \mid \Delta t < t_0)$ gives the probability that two consecutive avalanches separated by a Δt shorter than t_0 are such that $\Delta s < s_0$,

with s_0 a positive or negative integer. The conditional probability assesses the monotonic relation between consecutive avalanches as a function of the quiet time separating them, thus, providing a detailed picture of the correlation landscape of the avalanche process. To measure the strength and significance of such a relationship, for each given couple of thresholds s_0 and t_0, $P(\Delta s < s_0 \mid \Delta t < t_0)$ is systematically compared with the same conditional probability evaluated over 10^4 independent surrogate avalanche time series. Surrogates are obtained by randomly reshuffling avalanche sizes while keeping fixed their starting and ending times. $P(\Delta s < s_0 \mid \Delta t < t_0)$ are then compared with the average surrogate conditional probabilities, $P^*(\Delta s < s_0 | \Delta t < t_0)$, by analyzing the quantity

$$\delta P(s_0, t_0) \equiv P(\Delta s < s_0 \mid \Delta t < t_0) - P^*(\Delta s < s_0 \mid \Delta t < t_0)$$

as a function of s_0 for different fixed values of t_0 (Figure 3). Being $\sigma^*(s_0, t_0)$ the standard deviation of the surrogate conditional probability $P^*(\Delta s < s_0 | \Delta t < t_0)$, if $|\delta P(s_0,t_0)| > 2\sigma^*(s_0,t_0)$, one can conclude that P and P^* are significantly different (0.05 significance level), and that significant correlations exist between $\Delta s < s_0$ and $\Delta t < t_0$.

Two cases must be distinguished: $\delta P(s_0, t_0) > 0$ and $\delta P(s_0, t_0) < 0$. If $\delta P(s_0, t_0) > 0$, the number of avalanche couples $N(\Delta s < s_0, \Delta t < t_0)$ satisfying both conditions is significantly larger in the original data than in the surrogates; namely, it is more likely to find couples satisfying both conditions in the original rather than in the surrogate avalanche time series. Hence, Δs and Δt are positively correlated. On the contrary, if $\delta P(s_0,t_0) < 0$, the number of couples $N(\Delta s < s_0, \Delta t < t_0)$ satisfying both conditions is significantly larger in the surrogates than in the original data; namely, it is more likely to find couples satisfying both conditions in the uncorrelated surrogates rather than in the real avalanche time series. In this case, one says that Δs and Δt are negatively correlated.

Omori law

The number of avalanches per unit time, $N(t)$, occurring after a time t has elapsed from the main avalanche A^* is computed using a time window δt that increases logarithmically. Denoting a set of window boundaries as $W = (w_1, w_2, \ldots, w_k)$ and fixing $w_1 = 10$ ms, the logarithmic windows fulfill the relation $w_{i+1} = w_i \cdot 10^c$, which implies that the window size is constant in logarithmic scale, i.e., $log\ w_{i+1} - log\ w_i = c$. The following window sizes of c have been used in this study: $c = 0.1$ for the $N(t)$ of the awake resting state (Figures 3 and S9); $c = 0.11$ for the $N(t)$ during sleep (Figure 4).

Spearman's correlation coefficient

Given two variables X and Y, the Spearman's correlation coefficient is defined as

$$\rho_s = \frac{cov(rg_X, rg_Y)}{\sigma_{rg_X}\sigma_{rg_Y}},$$

where rg_X and rg_Y are the tied rankings of X and Y, respectively, σ_{rg_X} and σ_{rg_Y} their standard deviations, and $cov(rg_X, rg_Y)$ indicates the covariance between rg_X and rg_Y.

Surrogate signals

Surrogate signals are obtained by random phase shuffling of the original continuous signals. A Fourier transform of each sensor signal is performed, and the corresponding phases are randomized while amplitudes are preserved. The surrogate signals are then obtained by performing an inverse Fourier transform. The random phase shuffling destroys phase synchronization across cortical sites while preserving the linear properties of the original signals, such as power spectral density and two-point correlations.[84] Surrogate signals were used to generate surrogate data for Figures 2, 4, and 5.

Surrogate time series for correlations between Δs and Δt

To test significance of correlations between consecutive Δs and Δt, a surrogate sequence of avalanche sizes was generated for each subject by randomly reshuffling the original order of avalanche sizes. The Spearman's correlation coefficient $\rho(\Delta s, \Delta t)$ between consecutive Δs and Δt was calculated for each surrogate. The average Spearman's correlation coefficient obtained from all surrogates was then compared with the average correlation coefficient calculated from the original sequences of avalanche sizes and quiet times (Figures 1 and 4).

QUANTIFICATION AND STATISTICAL ANALYSIS

Power law exponents were estimated using a maximum likelihood estimator.[44,45,85] The power law fit was compared to an exponential fit by evaluating the log likelihood ratio $R = ln\ L_p/L_e$, where $L_{p,e} = \prod_{i=1}^{n} p_{p,e}(x_i)$ is the likelihood. R is positive if the data are more likely to follow a power law distribution, and negative if the data are more likely to follow exponential distribution. The statistical significance for R was estimated as in[44,85]. Following,[85] the p value associated to R is given by

$$p = \left|\mathrm{erfc}\left(R \Big/ \sqrt{2n}\,\sigma\right)\right|,$$

where σ^2 is the variance of the data[85] and

$$\mathrm{erfc}(z) = 1 - \mathrm{erf} = \frac{2}{\sqrt{\pi}}\int_z^{\infty} e^{-t^2 dt}$$

is the complementary Gaussian error function.[85]

Power-law exponent and fitting parameters for quiet time distributions, $P(\Delta t)$, for the autocorrelation $C(t)$, and for the function $N(t)$ were evaluated on pooled data, unless otherwise stated (Figures 1, 3, and 4). The corresponding error reported in the main text and in the figure caption is the error on the fit, unless otherwise stated.

Within each data group (MEG, EEG resting wake, EEG sleep), the Spearman's correlation coefficients $\rho(\Delta s, \Delta t)$ were evaluated for each subject. The values reported in the main text and in the figure captions are (mean $\pm$ SD) (Figures 1 and 4). Significance of correlations was assessed comparing the average correlation coefficient calculated from the original sequences of avalanche sizes and quiet times with the correlation coefficient calculated from surrogate time series (Figures 1 and 4). Pairwise comparisons were conducted using two-tailed Student's *t*-test.